1	Bacteriogenic Synthesis of Morphologically Diverse Silver Nanoparticles	
2	and their Assessment for Methyl Orange dye removal and antimicrobial	
3	activity	
4	Bhakti Patel ^{1†} , Virendra Kumar Yadav ^{1†} , Reema Desai ¹ , Shreya Patel ¹ , Abdelfattah	
5	Amari², Nisha Choudhary¹, Haitham Osman², Rajat Patel¹, Deepak Balram³, Kuang-Yow	
6	Lian ³ , Dipak Kumar Sahoo ^{4*} , and Ashish Patel ^{1*}	
7	¹ Department of Life Sciences, Hemchandracharya North Gujarat University, Patan	
8	384265, Gujarat, India	
9	² Department of Chemical Engineering, College of Engineering, King Khalid University,	
10	Abha 61411, Kingdom of Saudi Arabia	
11	³ Department of Electrical Engineering, National Taipei University of Technology, No. 1,	
12	Section 3, Zhongxiao East Road, Taipei 106, Taiwan	
13	⁴ Department of Veterinary Clinical Sciences, College of Veterinary Medicine, Iowa State	
14	University, Ames, Iowa, USA	
15 16 17 18 19	Correspondence: dsahoo@iastate.edu (D.K.S.); uni.ashish@gmail.com (A.P.)	Formatted: Font: (Default) Times New Roman
		Formatted: Font: (Default) Times New Roman Formatted: Font: (Default) Times New Roman
21	† These authors contributed equally to this work.	

Abstract

23

39 40

41 42

43

44

45

46

In the last decade nanotechnology and nanoparticles have attracted the attention of the scientific 24 community in the whole world. The microbial approaches for the synthesis of nanoparticles 25 are more economical, biocompatible, and environment-friendly than the chemical and physical 26 approaches. In the present research work, investigators have synthesized three different types 27 of silver nanoparticles (AgNPs), namely AgNPs-K, AgNPs-M, and AgNPs-E, by using 28 29 Klebsiella pneumoniae, Micrococcus luteus, and Enterobacter aerogenes, respectively. The 30 morphological, chemical, and elemental features of the synthesized AgNPs were analyzed by using UV-Vis spectroscopy (UV-Vis), Fourier transform-infrared spectroscopy (FTIR), X-ray 31 32 diffraction (XRD), field emission scanning electron microscope (FESEM) and energydispersive spectroscopy (EDX). UV-Vis absorbance peaks were obtained at 475 nm, 428 nm, 33 and 503 nm for AgNPs synthesized by, K. pneumoniae, M. luteus, and E. aerogenes 34 35 respectively. The XRD showed the crystalline nature of the synthesized AgNPs, having peaks at 26.2°, 32.1°, and 47.2°, while the FTIR showed bands at 599 cm⁻¹, 963 cm⁻¹, 1693 cm⁻¹, 36 2299 cm⁻¹, 2891 cm⁻¹, and at 3780 cm⁻¹ for all the types of AgNPs. The FTIR indicated the 37 presence of attached biomolecules from bacteria with developed AgNPs. The size of the AgNPs 38

Deleted: the

Deleted: I

like structure. The percentage of Ag varied from 37.8% (wt.%) to 61.6% i.e., highest in AgNPs-K, and lowest in AgNPs-M. Further, all three types of AgNPs were evaluated for the removal of methyl orange dyes from the simulated wastewater where the highest dye removal percentage was 19.24% at 120 minutes by AgNPs-M. Finally, all three types of AgNPs were assessed for their potential for antibacterial activity against Gram-positive bacteria (*Bacillus subtilis, B. cereus*, and *B. megaterium*) and Gram-negative bacteria (*Enterococcus fecalis*), out of which the largest zone of inhibition was 12 mm against *B. megaterium* for the AgNPs-M.

varies from 10 nm to several microns while the shape varies from spherical to porous sheets-

KEYWORDS silver nanoparticle, methyl orange, bioremediation, antimicrobial, zone of 49 inhibition 50 1. Introduction 51 The rapid industrialization in India as well as in the whole world has increased the use of 52 different synthetic dyes (Wang et al., 2023a). Some of the dyes may cause harm to aquatic life 53 54 and cause diseases in living organisms (Patel et al., 2022). Dyes are mainly used in textile 55 industries for coloring fabric, so textile industrial wastewater acts as a major source of dye effluent (Al-Tohamy et al., 2022). The prolonged and continuous mixing of dye-laden water Deleted: 56 and dye effluents in the freshwater may lead to water pollution (Patel et al., 2022; Agarwal et 57 58 al., 2022). The consumption of dye-contaminated water may cause numerous diseases in 59 humans, like skin irritation and skin cancer, in the long term. Dyes present in textile effluent Deleted: . can be removed by using various chemical approaches like precipitation, coagulation (Yadav 60 61 et al., 2022b; Wang et al., 2023c), flocculation, membrane filtration (nanofiltration, ultrafiltration) (Wang et al., 2020; Chahar et al., 2023; Zhang et al., 2023), reverse osmosis, 62 adsorption, etc. (Robati et al., 2016). The biological methods involve the utilization of 63 Deleted: methods Deleted: involves 64 microorganisms (Gupta et al., 2022) for dye remediation, either in the natural sites or in the bioreactor in the laboratory (Das & Mishra, 2017; Singh et al., 2023). The biological approach 65 Formatted: Font: (Default) Times New Roman, 12 pt 66 also involves biosorbents for the remediation of dyes from wastewater (Cui et al., 2017; Modi 67 et al., 2023). Such processes are economical if the biosorbents are developed from agricultural waste, etc. All of these processes have certain advantages and disadvantages, but adsorption is 68 a very simple, effective, and economical approach. The adsorbent in the adsorption process 69 70 could be easily surface functionalized by various chemical compounds for the targeted removal of pollutants (Cui et al., 2013; Chen et al., 2020; Harja, Buema & Bucur, 2022). The various 71 72 adsorbents that are commonly used for the remediation of dyes and other pollutants from Deleted: which contaminated water are alumina, silica (Imoisili, Nwanna & Jen, 2022; Yadav et al., 2023), Deleted: water alumina 73

80	zeolites (Murukutti & Jena, 2022), coal fly ash, magnetite, maghemite, zinc oxide (Soltani et	
81	al., 2023), titanium dioxide (Dash et al., 2018; Yang, Shojaei & Shojaei, 2022), and other	 Deleted: and
82	complexes (Cui et al., 2017). When these adsorbents are used in their nanoform, they become	
83	highly effective due to their high surface area to volume ratio (SVR), and high surface energies	 Deleted: ,
84	(Chen et al., 2020).	
85	Nanotechnology has played a significant role in environmental clean-up, especially the	 Deleted: cleanup
86 86	removal of textile dyes from contaminated water. Among NPs, metallic, metal oxide NPs, and	
87	nanocomposites Among pure metallic NPs, silver nanoparticles (AgNPs) have gained huge	 Deleted: has
88	popularity as they are effective in killing waterborne pathogens due to their antimicrobial	 Deleted: it is
89	properties (Choudhary, Pathak & Madhusudan, 2017). The size of the NPs mainly falls in the	 Deleted: also Deleted: y
90	range of 1 to 100 nm (Puri, Gupta & Mishra, 2021), which has gained huge popularity in the	Deleted: y
91	field of adsorption-based removal of pollutants from wastewater due to their <u>SVR</u> . Moreover,	 Deleted: SVR
92	NPs have <u>a high</u> adsorption capacity, due to which dyes easily get adsorbed on the surface of	
93	NPs (Degefa et al., 2021; Tarekegn et al., 2021; Wang et al., 2023a),	 Deleted:
93 94	NPs (Degefa et al., 2021; Tarekegn et al., 2021; Wang et al., 2023a), AgNPs could be synthesized by all three possible methods, i.e., chemical, physical, and	 Deleted:
		 Deleted: Deleted: includes
94	AgNPs could be synthesized by all three possible methods, i.e., chemical, physical, and	
94 95	AgNPs could be synthesized by all three possible methods, i.e., chemical, physical, and biological (Bouafia et al., 2021). The chemical approaches include chemical coprecipitation	 Deleted: includes
94 95 96	AgNPs could be synthesized by all three possible methods, i.e., chemical, physical, and biological (Bouafia et al., 2021). The chemical approaches include chemical coprecipitation (Adibah, Firdianti & Suprapto, 2023), sol-gel (Shahjahan et al., 2017), chemical reduction	 Deleted: includes
94 95 96 97	AgNPs could be synthesized by all three possible methods, i.e., chemical, physical, and biological (Bouafia et al., 2021). The chemical approaches include chemical coprecipitation (Adibah, Firdianti & Suprapto, 2023), sol-gel (Shahjahan et al., 2017), chemical reduction (Horne et al., 2023), polyol (Wolf et al., 2022), etc. Among physical approaches, the most	Deleted: includes
94 95 96 97 98 99	AgNPs could be synthesized by all three possible methods, i.e., chemical, physical, and biological (Bouafia et al., 2021). The chemical approaches include chemical coprecipitation (Adibah, Firdianti & Suprapto, 2023), sol-gel (Shahjahan et al., 2017), chemical reduction (Horne et al., 2023), polyol (Wolf et al., 2022), etc. Among physical approaches, the most familiar ones are ball milling (Lai et al., 2023), the vapor condensation method (Simchi et al.,	Deleted: includes
94 95 96 97 98 99	AgNPs could be synthesized by all three possible methods, i.e., chemical, physical, and biological (Bouafia et al., 2021). The chemical approaches include chemical coprecipitation (Adibah, Firdianti & Suprapto, 2023), sol-gel (Shahjahan et al., 2017), chemical reduction (Horne et al., 2023), polyol (Wolf et al., 2022), etc. Among physical approaches, the most familiar ones are ball milling (Lai et al., 2023), the vapor condensation method (Simchi et al., 2007), arc discharge (El-Khatib et al., 2018), and laser-ablation techniques (Rafique et al.,	Deleted: includes Formatted: Font: (Default) Times New Roman, 12 pt Deleted: . Deleted: involves
94 95 96 97 98 99	AgNPs could be synthesized by all three possible methods, i.e., chemical, physical, and biological (Bouafia et al., 2021). The chemical approaches include chemical coprecipitation (Adibah, Firdianti & Suprapto, 2023), sol-gel (Shahjahan et al., 2017), chemical reduction (Horne et al., 2023), polyol (Wolf et al., 2022), etc. Among physical approaches, the most familiar ones are ball milling (Lai et al., 2023), the vapor condensation method (Simchi et al., 2007), arc discharge (El-Khatib et al., 2018), and laser-ablation techniques (Rafique et al., 2019; Juma et al., 2023). The chemical approaches involve the utilization of hazardous	Deleted: includes Formatted: Font: (Default) Times New Roman, 12 pt Deleted: .
94 95 96 97 98 99 100 101	AgNPs could be synthesized by all three possible methods, i.e., chemical, physical, and biological (Bouafia et al., 2021). The chemical approaches include chemical coprecipitation (Adibah, Firdianti & Suprapto, 2023), sol-gel (Shahjahan et al., 2017), chemical reduction (Horne et al., 2023), polyol (Wolf et al., 2022), etc. Among physical approaches, the most familiar ones are ball milling (Lai et al., 2023), the vapor condensation method (Simchi et al., 2007), arc discharge (El-Khatib et al., 2018), and laser-ablation techniques (Rafique et al., 2019; Juma et al., 2023). The chemical approaches involve the utilization of hazardous chemicals, which are not environmentally friendly, while the physical ones utilize of expensive	Deleted: includes Formatted: Font: (Default) Times New Roman, 12 pt Deleted: . Deleted: involves Deleted: environmental
94 95 96 97	AgNPs could be synthesized by all three possible methods, i.e., chemical, physical, and biological (Bouafia et al., 2021). The chemical approaches include chemical coprecipitation (Adibah, Firdianti & Suprapto, 2023), sol-gel (Shahjahan et al., 2017), chemical reduction (Horne et al., 2023), polyol (Wolf et al., 2022), etc. Among physical approaches, the most familiar ones are ball milling (Lai et al., 2023), the vapor condensation method (Simchi et al., 2007), arc discharge (El-Khatib et al., 2018), and laser-ablation techniques (Rafique et al., 2019; Juma et al., 2023), The chemical approaches involve the utilization of hazardous chemicals, which are not environmentally friendly, while the physical ones utilize of expensive instruments, which makes the synthesis highly expensive. The biological synthesis techniques.	Deleted: includes Formatted: Font: (Default) Times New Roman, 12 pt Deleted: . Deleted: involves Deleted: environmental

a chemical capping agent or surfactant. The microbial synthesis methods provide natural 120 Deleted: no requirement of chemical capping agent or 121 stabilizing and capping agents, which make them biocompatible (Naganthran et al., 2022). Among all the microorganisms, bacterial synthesis is preferred due to their easy handling and 122 Deleted: short time duration for their growth in comparison to algae and fungi (Wang et al., 2023b; 123 Choudhary et al., 2023b). Bacteria are enriched with several bacterial enzymes and proteins, 124 which play an important role in the bio-reduction of Ag²⁺ ions into Ag⁰. These biological 125 126 molecules act as reducing agents, capping agents, and stabilizing agents for the developed AgNPs. Vimalanathan and his team synthesised silver nanoparticles (AgNPs) using the moist 127 128 biomass of *Micrococcus luteus*, (Vimalanathan et al., 2013). To date a several investigators have Deleted: A team led by Vimalanathan synthesized AgNPs by using wet biomass of the Micrococcus luteus 129 used potential bacteria for the formation of AgNPs for instance, Esmail and his colleagues Formatted: Font: Italic Deleted: their team 130 synthesized AgNPs (25 nm), by using the supernatant of the bacteria Bacillus ROM6. This Deleted:),, particular bacterium was isolated from the Zarshouran gold mine in South Korea. Further, the Deleted: 131 132 synthesized AgNPs were used as an antimicrobial agent against Escherichia coli, Acinetobacter baumannii, Staphylococcus aureus, and Pseudomonas aeruginosa (Esmail et al., 2022). 133 134 From the very beginning of civilization, the antimicrobial effect of Agwas known due to which Deleted: is 135 it was used for various applications (Kyung et al., 2008). Being a heavy metal, it coagulates 136 the enzymes and proteins of the microorganism, thus inhibiting them and ultimately killing 137 them (Betts, Whitehead & Harris, 2021). So, the nanosized silver can increase the efficiency 138 of antimicrobial activity due to its small size, and high SVR, as it is smaller in size, it may enter Commented [GR1]: Font type Deleted: high SVR the microorganism through the cell wall, resulting in the inhibition and killing of the 139 Deleted: as being smaller in size 140 microorganism (Karunakaran et al., 2017). Several research studies have revealed that the AgNPs possess incredible antimicrobial activity, (Singh & Mijakovic, 2022) which depends Deleted: 141 upon their size and surface area (Kalwar & Shan, 2018). The smaller size of AgNPs may Deleted: 142 Deleted: inside 143 facilitate their entry into the microbes and exhibit their antimicrobial effect. There are several examples where AgNPs have been used as an antimicrobial agent. 144

159	Saeed and co-researchers synthesized spherical-shaped AgNPs of size 5-50 nm using bacterial		
160	strains; E. coli, Exiguobacterium aurantiacumm, and Brevundimonas diminuta. The		
161	investigators further, observed the antimicrobial activity of the synthesized AgNPs against		
162	methicillin-resistant Staphylococcus aureus (MRSA) and several other multiple drug resistance		
163	(MDR) bacteria, where the zone of inhibition (ZOI) varied from 10 mm to 28 mm. Further, the	(Deleted: was varying
164	investigators utilized AgNPs against plant pathogens (Saeed, Iqbal & Ashraf, 2020). Agesearch	(Deleted: team
165	group led by Cekuolyte synthesized morphologically different types of AgNPs by using		
166	different strains of <i>Geobacillus</i> bacteria, namely, 18, 25, 95, and 612 (Cekuolyte et al., 2023).	(Deleted: ,
167	Aresearch group led by Raza synthesized AgNPs by using Aspergillus fumigatus KIBGE-IB33	(Deleted: team
168	and evaluated the antimicrobial activity of AgNPs on Enterococcus faecalis ATCC 29212.	(Deleted: the
169	Further, the investigators developed a nanocomposite by using the AgNPs with chitosan and		
170	observed that the lowest minimum inhibitory concentration of the nanocomposite system was		
171	1.56 μg mL ⁻¹ against <i>Enterococcus faecalis</i> ATCC 29212 (Raza et al., 2021). Srinivasan and		
172	their colleagues synthesised silver nanoparticles (AgNPs) using a bioluminescent bacterium	(Commented [GR2]:his colleagues
	their colleagues synthesised silver nanoparticles (AgNPs) using a bioluminescent bacterium (Vibrio campbellii).		Commented [GR2]:his colleagues Deleted: Srinivasan and their team, synthesized AgNPs by using a bioluminescent bacterium
172 173	(Vibrio campbellii),		Deleted: Srinivasan and their team, synthesized AgNPs by
172 173 174	(Vibrio campbellii). Further, the investigators assessed the antibacterial and antioxidant properties of the		Deleted: Srinivasan and their team, synthesized AgNPs by using a bioluminescent bacterium
172 173	(Vibrio campbellii),		Deleted: Srinivasan and their team, synthesized AgNPs by using a bioluminescent bacterium
172 173 174	(Vibrio campbellii). Further, the investigators assessed the antibacterial and antioxidant properties of the		Deleted: Srinivasan and their team, synthesized AgNPs by using a bioluminescent bacterium
172 173 174 175	(Vibrio campbellii). Further, the investigators assessed the antibacterial and antioxidant properties of the synthesized AgNPs. The antibacterial potential was evaluated against several pathogenic		Deleted: Srinivasan and their team, synthesized AgNPs by using a bioluminescent bacterium
172 173 174 175 176	(Vibrio campbellii). Further, the investigators assessed the antibacterial and antioxidant properties of the synthesized AgNPs. The antibacterial potential was evaluated against several pathogenic Gram-negative bacteria (GNB) like Aeromonas hydrophila MTCC		Deleted: Srinivasan and their team, synthesized AgNPs by using a bioluminescent bacterium
172 173 174 175 176	(Vibrio campbellii). Further, the investigators assessed the antibacterial and antioxidant properties of the synthesized AgNPs. The antibacterial potential was evaluated against several pathogenic Gram-negative bacteria (GNB) like Aeromonas hydrophila MTCC 1739, Klebsiella oxytoca MTCC 3030, K. pneumoniae MTCC4030,		Deleted: Srinivasan and their team, synthesized AgNPs by using a bioluminescent bacterium Deleted:
172 173 174 175 176 177	Further, the investigators assessed the antibacterial and antioxidant properties of the synthesized AgNPs. The antibacterial potential was evaluated against several pathogenic Gram-negative bacteria (GNB) like <i>Aeromonas hydrophila</i> MTCC 1739, <i>Klebsiella oxytoca</i> MTCC 3030, <i>K. pneumoniae</i> MTCC4030, and <i>Ps. aeruginosa</i> MTCC 1934. The AgNPs exhibited antioxidant features through strong		Deleted: Srinivasan and their team, synthesized AgNPs by using a bioluminescent bacterium Deleted: Deleted: by
172 173 174 175 176 177 178	Further, the investigators assessed the antibacterial and antioxidant properties of the synthesized AgNPs. The antibacterial potential was evaluated against several pathogenic Gram-negative bacteria (GNB) like <i>Aeromonas hydrophila</i> MTCC 1739, <i>Klebsiella oxytoca</i> MTCC 3030, <i>K. pneumoniae</i> MTCC4030, and <i>Ps. aeruginosa</i> MTCC 1934. The AgNPs exhibited antioxidant features through strong scavenging actions on 2,2-diphenyl-1-picrylhydrazyl (DPPH) (61.88%) and H ₂ O ₂ (53.48%)		Deleted: Srinivasan and their team, synthesized AgNPs by using a bioluminescent bacterium Deleted: Deleted: by
172 173 174 175 176 177 178 179 180	Further, the investigators assessed the antibacterial and antioxidant properties of the synthesized AgNPs. The antibacterial potential was evaluated against several pathogenic Gram-negative bacteria (GNB) like <i>Aeromonas hydrophila</i> MTCC 1739, <i>Klebsiella oxytoca</i> MTCC 3030, <i>K. pneumoniae</i> MTCC4030, and <i>Ps. aeruginosa</i> MTCC 1934. The AgNPs exhibited antioxidant features through strong scavenging actions on 2,2-diphenyl-1-picrylhydrazyl (DPPH) (61.88%) and H ₂ O ₂ (53.48%) free radicals (Srinivasan et al., 2022). From the above investigation, it was found that there was		Deleted: Srinivasan and their team, synthesized AgNPs by using a bioluminescent bacterium Deleted: Deleted: by
172 173 174 175 176 177 178 179 180	Further, the investigators assessed the antibacterial and antioxidant properties of the synthesized AgNPs. The antibacterial potential was evaluated against several pathogenic Gram-negative bacteria (GNB) like <i>Aeromonas hydrophila</i> MTCC 1739, <i>Klebsiella oxytoca</i> MTCC 3030, <i>K. pneumoniae</i> MTCC4030, and <i>Ps. aeruginosa</i> MTCC 1934. The AgNPs exhibited antioxidant features through strong scavenging actions on 2,2-diphenyl-1-picrylhydrazyl (DPPH) (61.88%) and H ₂ O ₂ (53.48%) free radicals (Srinivasan et al., 2022). From the above investigation, it was found that there was no information on the morphology of AgNPs synthesized by different bacteria. Moreover,		Deleted: Srinivasan and their team, synthesized AgNPs by using a bioluminescent bacterium Deleted: Deleted: by Deleted: and

195	purity. Moreover, the antimicrobial effect of morphologically diverse AgNPs on the pathogenic		Commented [GR3]: Font type
196	bacteria.	- Tables of	Deleted: So, a study is needed to investigate the effect on the morphology of AgNPs and purity by different bacteria.
197	From all the above investigations, various gaps were found, which are mentioned below: i) the		
198	effect of different bacterial strains and their enzymes on the morphology of the synthesis of		
199	AgNPs: ii) the utilization of AgNPs along with composite material to form nanocomposite for		Deleted: ,
200	antimicrobial properties, could not reveal the effectiveness of the antimicrobial properties of	<	Deleted: y
201	AgNPs in the composite. So, to understand these two above-mentioned issues, a detailed	1/3	Deleted: ed
202	investigation is needed to study the effect on the morphology of AgNPs and their purity by	Y	Deleted: property
203	different bacteria and their enzymes, as well as the antimicrobial potential effect of		Deleted: and
204	morphologically diverse AgNPs on the pathogenic GPB and GNB.		
205	Gola and their group synthesized 6-25 nm, spherical, and hexagonal-shaped AgNPs from		
206	Aspergillus sps. Further, the synthesized AgNPs were used for the removal of reactive yellow		
207	dye and antibacterial potential (Gola et al., 2021). A research group led by Rasheed, synthesized		Deleted: and their team
208	AgNPs from Conocarpus erectus and Pseudomonas sp. and applied them to the elimination of		Deleted: for
209	reactive black 5 (RR5) and reactive red 120 (RR120) from the aqueous solutions (Rasheed et		Deleted:) from
210	al., 2023).		
211	Here, the investigators have harnessed the potential of Gram-positive bacteria (Micrococcus		
212	luteus) and Gram-negative bacteria (Klebsiella pneumoniae and Enterobacter aerogenes) for		
213	the synthesis of silver nanoparticles (AgNPs) under normal laboratory conditions. One of the		
214	objectives was to confirm the formation of AgNPs, along with purity and morphology, by using		
215	Fourier transform-infrared (FTR-IR), UV-Vis spectrophotometer (UV-Vis), X-ray diffraction		
216	pattern (XRD), Field emission scanning electron microscopy (FESEM), and Energy dispersive		
217	X-ray spectroscopy (EDS). AgNPs. Another objective was to observe the morphological and		
218	elemental diversity among the bacterially synthesized AgNPs. Another objective was to		

evaluate the potential of AgNPs as an adsorbent for the removal of methyl orange dye from Deleted: the 230 aqueous solutions. The final objective was to evaluate the potential of the synthesized AgNPs 231 as an antibacterial agent against GPB (B. subtilis, B. cereus, and B. megaterium) and GNB 232 (Enterococcus fecalis). 233 2. Materials and methods 234 235 2.1. Materials 236 K. pneumoniae, M. luteus, E. aerogenes, B. subtilis, B. cereus, B. megaterium, and Deleted: and 237 Enterococcus fecalis were procured from the Gujarat Biotech Research Centre, Gujarat, India, silver nitrate (SRL, Gujarat, India), nutrient agar media (Himedia, Mumbai, India); nutrient Deleted: , 238 Deleted:), 239 broth (Himedia, Gujarat, India); antibiotic assay media (Himedia, Mumbai, India); ethanol Deleted:), 240 (Shenzhen, China), Whatman filter paper no. 42. (Axiva, Mumbai, India); and methyl orange Deleted: E Deleted:), (Loba, Chemie, Gujarat, India). All the chemicals were of analytical grade except silver nitrate 241 242 and methyl orange dye (LR grade) and double distilled water (ddw). Deleted: 2.2. Methods 243 2.2.1. Screening and selection of bacteria for the synthesis of AgNPs 244 245 Around 10 bacterial colonies were procured on nutrient agar Petri plates, which were stored in 246 a refrigerator in the laboratory. Further, about 200 mL of nutrient broth was prepared, to which about 1 mM of an aqueous solution of AgNO3 was added. Further, about 10 mL of this mixture 247 248 was transferred into 10 different Erlenmeyer flasks of 50 mL. To all these flasks, a loopful culture of each bacterial strain was added and incubated in an incubator shaker at 37 °C for 2-249 250 3 days. After incubation, a color change was noticed, and later on, UV-Vis spectra were taken 251 for all the samples. Out of all these bacterial strains, only three were found positive for the AgNPs synthesis as the color change to red and an absorbance peak near 500-540 nm was 252 253 observed. So further, only these three bacterial strains were used for the large amount of AgNPs

formation. These bacterial strains were identified by 168 rRNA genome sequencing. The Deleted: 16s 262 263 selected bacterial strains were M. luteus, K. pneumoniae, and E. aerogenes. 2.2.2. Synthesis of silver nanoparticles from bacteria 264 For the fabrication of AgNPs, silver salt was reduced by the bacterial supernatants obtained 265 266 from all three bacterial strains. The isolated bacterial colonies were grown on nutrient agar 267 plates. Further, for the mass production of each bacterial colony, a loopful of culture was 268 inoculated into the nutrient broth in three separate Erlenmeyer flasks. All three flasks Deleted: taken containing nutrient broth were incubated in an incubator shaker at 37 °C for 24 hours at 120 269 270 rpm. Further, after 24 hours, the bacterial colonies were taken out and centrifuged at 5000 rpm 271 for 10 minutes. The bacterial supernatant was retained, while the bacterial pellet was discarded. 272 Further, about 100 mL of all three bacterial supernatants were taken separately in three amber bottles, and to each bottle, about 100 mL of silver nitrate solution was added. After that, all 273 274 three flasks, including the control, which has ddw instead of bacterial supernatant, were kept 275 under dark conditions for 2-3 days, and color change was continuously monitored. Initially, the 276 color of the silver nitrate aqueous solution was pale, but after the addition of bacterial Deleted: while. 277 supernatant, the color tuned to a milky white in appearance. Finally, after 2-3 days, the color of the three bottles changed from milky white to reddish brown, indicating the formation of 278 279 AgNPs. The mixture from each bottle was transferred to the centrifugation tubes separately and 280 centrifuged at 5000 rpm for 10 minutes. The supernatant was discarded, while the solid particle was retained. Further, the pellet was washed 2-3 times with distilled water and once with 281 ethanol. All three types of AgNPs were then transferred to different Petri plates and kept for Deleted: into 282 drying in an oven at 50-60 °C untill complete dryness. Figure 1 shows the schematic steps 283

FIGURE 1 Schematic diagram for the synthesis of AgNPs using bacterial supernatant. The first step involves the growth of bacterial culture. The second step involves the lysis of the Deleted: gro bacterial cells by centrifugation. The third step involves the addition of silver ion precursors Deleted: s to all the bacterial supernatant. The fourth step involves color change observation and Deleted: in confirmation by UV-Vis. The final step involves the recovery, washing, and drying of the AgNPs. 288 involved in the development of AgNPs from the bacterial supernatant, 2.2.3. Preparation of Deleted: ¶ aqueous solution methyl orange dye Deleted: ¶ 289 A 50-ppm aqueous solution of methyl orange (MO) dye was prepared by adding 50 mg of MO 290 291 dye powder granules into the 1000 mL ddw. The aqueous solution was kept on a magnetic stirrer with vigorous stirring at 250 rpm to completely dissolve the dye granules. Further, 292 Deleted: along Whatman filter paper was used for the filtration of the aqueous solution to eliminate the 293 Deleted: a 294 impurities. Finally, the dye sample was placed in an amber-colored glass reagent bottle for future use. 295 2.2.4. Batch study of adsorption of methyl orange dye 296 297 About 100 mL of an aqueous solution of MO dye was taken from the stock solution into three different glass beakers of appropriate volume. All three glass beakers were placed on a 298 Deleted: these magnetic stirrer, and 1 mg of AgNPs of each type was added to different glass beakers. The Deleted: to which 299 interaction between the AgNPs and MO dye was carried out by agitation at 400 rpm for all 300 three flasks. Further, an aliquot (2-3 mL) was collected from all three glass beakers at 0 301 302 minutes, 30, 60, 90, and 120 minutes. All the collected samples were then analyzed by the UV-Deleted: minutes Deleted: minutes 303 Vis spectrophotometer to identify the concentration of the dye samples. The UV-Vis Deleted: concentration 304 absorbance maxima of MO dye are 520±15 nm. Further, MO dye removal percentage was

measured by using the following formula as provided by (Swathilakshmi et al., 2022) in 319 Equation (1): 320 Deleted:): Deleted: % Dye removal = $\frac{Co - Ct}{Co} \times 100$ (1) 321 322 Where, C_o= initial dye concentration, 323 Ct= dye concentration at a specific time 324 2.2.5. Antimicrobial activity of silver nanoparticles 325 The antimicrobial properties of all the bacterially developed AgNPs (AgNPs-K, AgNPs-M, and 326 Deleted: property AgNPs-E) were assessed against GPB: B. subtilis, B. cereus, B. megaterium, and GNB: E. 327 Deleted: was 328 faecalis by the disc diffusion method (Yassin et al., 2022). Firstly, 16 discs of specific size (8 Deleted: disk Deleted: disks mm diameter) were cut out of filter paper and dipped into separate reagent vials containing 329 AgNPs-K, AgNPs-M, and AgNPs-E. Further, all the reagent vials were sonicated for 15-20 330 331 minutes using an ultrasonicator (Lequitron). Further, the AgNPs loaded discs were taken out of Deleted: disks 332 the vials with the help of forceps kept on three different Petri plates and dried in a hot air oven Deleted: in Deleted: at 40-50 °C. Further, autoclaved antibiotic assay media was prepared, in which all four tested 333 Deleted: to 334 bacteria were spread with the help of a sterilized cotton swab on different plates under aseptic Deleted: was Deleted: . 335 conditions. The dried AgNPs loaded discs (three disks in one plate) were gently placed on the Deleted: disks bacteria-swabbed Petri plates. Finally, the Petri plates were incubated overnight in a bacterial Deleted: for 336 incubator at 37 °C. After 24 hours, antibiotic assay plates were observed for the evaluation of 337 the antimicrobial features of the formulated AgNPs. The ZOI was measured by using a 338 measurement scale against the light, and the size was recorded in mm (Ballén et al., 2021). 339 3. Characterization of silver nanoparticles 340 341 3.1. UV-Visible spectroscopy

356	The UV-Vis measurement of AgNPs was done by dispersing about 1 mg of all three types of	
357	AgNPs in 5 mL of ddw in three different test tubes. All three tubes containing AgNPs were	Deleted: having
 358	sonicated in an ultrasonicator for 10 minutes to disperse the particles. The well-dispersed	
359	samples were then taken in a quartz cuvette, and the UV-Vis measurement was done in the	
360	range of 200-800 nm at a resolution of 1 nm, by using a UV-Vis spectrophotometer (UV 1800,	Deleted: ,
361	Shimadzu spectrophotometer, Japan).	
362	3.2. FTIR	
363	The FTIR measurement was done to identify the various functional groups present in the	
364	bacterially synthesized AgNPs. The FTIR measurement was done using the solid KBr pellet	Deleted: by
365	method, where the pellets were prepared by mixing 2 mg AgNPs and 198 mg KBr for all three	Deleted: where the
366	types of AgNPs. The measurement was done in the mid-IR region $599-4000\ cm^{-1}$ at a resolution	Deleted: the
367	of 2 cm ⁻¹ by using a spectrum S6500 instrument (Perkin-Elmer, USA).	
368	3.3. XRD	
369	The XRD patterns for all three types of AgNPs samples were recorded using a Miniflex 800	Deleted: by
370	(Rigaku, Netherlands) instrument equipped with an X'celerometer to reveal the	
371	crystallinity. XRD patterns were recorded in the 2-theta range of 20-70 by using a filter K-beta	
372		
	(x1) with a step size of 0.02 and a time of 5 seconds per step, scan speed/duration time: 10.0	
373	(x1) with a step size of 0.02 and a time of 5 seconds per step, scan speed/duration time: 10.0 degree/min., step width: 0.0200 degree at 30 kV voltage, and a current of 2 mA.	
373 374		
	degree/min., step width: 0.0200 degree at 30 kV voltage, and a current of 2 mA.	Deleted: out by
374	degree/min., step width: 0.0200 degree at 30 kV voltage, and a current of 2 mA. 3.4. FESEM-EDS	Deleted: out by
374 375	degree/min., step width: 0.0200 degree at 30 kV voltage, and a current of 2 mA. 3.4. FESEM-EDS The morphological analysis of all three types of AgNPs was investigated using a Novo	Deleted: out by Deleted: for
374 375 376	degree/min., step width: 0.0200 degree at 30 kV voltage, and a current of 2 mA. 3.4. FESEM-EDS The morphological analysis of all three types of AgNPs was investigated using a Novo Nanosem, Fei 450, (USA). The dry AgNPs were loaded on the carbon tape with the help of a	
374 375 376 377	degree/min., step width: 0.0200 degree at 30 kV voltage, and a current of 2 mA. 3.4. FESEM-EDS The morphological analysis of all three types of AgNPs was investigated using a Novo Nanosem, Fei 450, (USA). The dry AgNPs were loaded on the carbon tape with the help of a fine brush, which in turn was kept on the Al stub holder. All the samples were exposed to gold	Deleted: for
374 375 376	degree/min., step width: 0.0200 degree at 30 kV voltage, and a current of 2 mA. 3.4. FESEM-EDS The morphological analysis of all three types of AgNPs was investigated using a Novo Nanosem, Fei 450, (USA). The dry AgNPs were loaded on the carbon tape with the help of a fine brush, which in turn was kept on the Al stub holder. All the samples were exposed to gold	Deleted: for

dispersive X-ray spectroscopy (EDS) analyzer fixed to the FESEM at variable magnifications 388 at 20 kV. 389 4. Results and discussion 390 4.1. Mechanism of formation of AgNPs by bacteria 391 392 The bacterial strains, i.e., K. pneumoniae, M. luteus, and E. aerogenes, have numerous Formatted: Font: Not Italic microbial proteins and enzymes that help in the bioreduction of Ag2+ ions into Ag0 (Ballén et 393 394 al., 2021). The actual mechanism of the biosynthesis of AgNPs by bacteria is well described in 395 the literature. It is a very simple and easy mechanism where the oxidized silver ions get two electrons from any of the microbial proteins and enzymes and get reduced to the stabilized Ag⁰. 396 When the AgNO₃ aqueous solutions are mixed with the bacterial culture/supernatant, the 397 bacterial enzymes present in the supernatant reduce the Ag²⁺ ions into Ag⁰. So, during this step, 398 Deleted: 0.. the previously milky color of the aqueous silver solutions gets converted to a red color, which 399 indicates the development of AgNPs in the medium. Moreover, these biomolecules may also 400 act as stabilizing and capping agents for the synthesized AgNPs (Giri et al., 2022; Terzioğlu et 401 al., 2022). Figure 2 shows the mechanism involved in the formation of AgNPs from the 402 403 bacteria. Here, the color of the medium changed from milky white to dark brown within 2-3 days. Earlier, a similar color change (yellow to brown) was observed during the synthesis of 404 Deleted: lso 405 AgNPs by K. pneumoniae isolated from humans and sheep (Sayyid & Zghair, 2021). Saleh and 406 Alwan (2020) used K. pneumoniae culture supernatant for the biosynthesis of AgNPs (Saleh & 407 Khoman Alwan, 2020). Earlier, Javaid et al. also suggested a similar pathway for the formation Deleted: and their group of AgNPs from the bacteria via a NADH-dependent nitrate reductase enzyme (Javaid et al., 408 409 2018). Table 1 shows the major microbial proteins and enzymes present in K. pneumoniae, M. Deleted: is showing 410 luteus, and E. aerogenes.

TABLE 1 The major microbial proteins and enzymes present in K. pneumoniae, M. luteus,

can be obtained when more amount of cultural filtrate is used. The investigator further showed that the amount of reducing agents plays an important role in the formation of AgNPs (Kalpana

416 and E. aerogenes.

FIGURE 2 Schematic diagram for the development of AgNPs from silver ions by bacteria via the NADH-dependent nitrate reductase enzyme. The oxidized silver ions interact with the bacterial NADPH-dependent nitrate reductase enzyme, leading to the reduction of the Ag²⁺ ions. The silver ions get capped with biomolecules from the bacteria. Further, these silver ions grow and nucleate,

which get capped and stabilized by bacterial biomolecules, leading to the formation of stabilize Deleted: s

AgNPs.

417

431

432

433

& Lee, 2013).

415

418 4.2. UV-Vis analysis for preliminary confirmation of the formation of AgNPs Deleted: ¶ 419 Figure 3 shows the typical UV-Vis spectra of AgNPs synthesized by bacteria. All of them exhibit a peak in the range of 425-505 nm. These absorbance peaks indicate the formation of 420 AgNPs from the Ag2+ ions by the bacteria (Saleh & Khoman Alwan, 2020). Earlier, Saleh and 421 Alwan (2020) obtained a peak at 432 nm for the AgNPs synthesized by K. pneumoniae (Saleh 422 & Khoman Alwan, 2020), 420 and 440 nm by M. luteus (Vimalanathan et al., 2013), 450 nm 423 424 by cyanobacterium Oscillatoria limnetica (Hamouda et al., 2019), 450 nm by endophytic Deleted: a Deleted: the bacteria Enterobacter roggenkampii BLS02 (Kumar & Dubey, 2022), and 405-407 nm for 425 426 Klebsiella pneumoniae by the research group of Kalpana. The investigators concluded that Deleted: and their team Deleted: 427 when the ratio of AgNO₃ to bacterial supernatant was about 4:6, the absorption intensity was Deleted: Deleted: then higher, so they formed AgNPs. It was further concluded that the UV-Vis absorption is directly 428 Deleted: Further proportional to the amount of substance at their maximum absorption spectra, i.e., a higher 429 430 yield of AgNPs and efficient production of AgNPs even at lower concentrations of silver nitrate

Deleted: also

FIGURE 3 UV-Vis measurement of AgNPs synthesized by bacteria.

4.3. Identification of functional groups of silver NPs by FTIR

461 A typical FTIR spectra of all the AgNPs (AgNPs-K, AgNPs-M, and AgNPs-E) synthesized by

462 bacteria is shown in Figure 4 which was used for the identification of various functional

groups present in AgNPs. All the samples have a common band at 599 cm⁻¹ and 963, 1299,

464 1349, 1693, 2299, 2891, and 3780 cm⁻¹. The band at 599 cm⁻¹ is attributed to the metallic Ag.

The band at 963 cm⁻¹ is attributed to the amide V band arising due to out-of-plane NH bending

of peptide linkages (Kalpana & Lee, 2013). A small intensity band at 1051 cm⁻¹ is attributed

to the primary amine C-N stretch. Another small intensity band at 1349 cm⁻¹ in all the samples

is attributed to the C-C bond. A small intensity band in all the samples at 1699 cm⁻¹ is attributed

to the OH group in the samples. Moreover, this band is also attributed to the C=O stretching of

amide I bands of peptide linkage. The band at 1229 cm⁻¹ is attributed to the CN stretching of

peptide linkage. The band at 1349 cm⁻¹ is attributed to the (C-C) stretching vibration of

aliphatic amines, which was previously documented by Ibrahim and their research group. In

their study, the investigators developed AgNPs from endophytic bacteria, which showed a

FTIR band at 1359 cm⁻¹ (Ibrahim et al., 2019). All the samples exhibit an atmospheric carbon

band at 2891 cm⁻¹ is attributed to the methylene C–H asymmetric or symmetric stretch. All the

samples showing a small band from 3400 cm⁻¹ to 3800 cm⁻¹ centred at 3780 cm⁻¹ are attributed

to the -OH molecule.

459

460

466

467

468

469

470

471

473

474

475

476

477

478

479

480

481

482

483

Earlier, Saleh and Alwan (2020) obtained four distinct peaks for the AgNPs synthesized by K.

pneumoniae at 3332.78 cm⁻¹, 2115.35, 1635.60, and 1096.92 cm⁻¹. The investigators

concluded that the band obtained at 3332.78 cm⁻¹-is due to the stretching vibration of the OH

bond of alcohol and phenols. The band at 2115.35 cm⁻¹ was found due to the C-H stretching of

the methylene groups of protein and to the N-H stretching of amine salt. The band at 1635.60

cm⁻¹ was attributed to the carbonyl groups (C=O) of the amino acid residues, while the band at

Formatted: Font: Not Bold

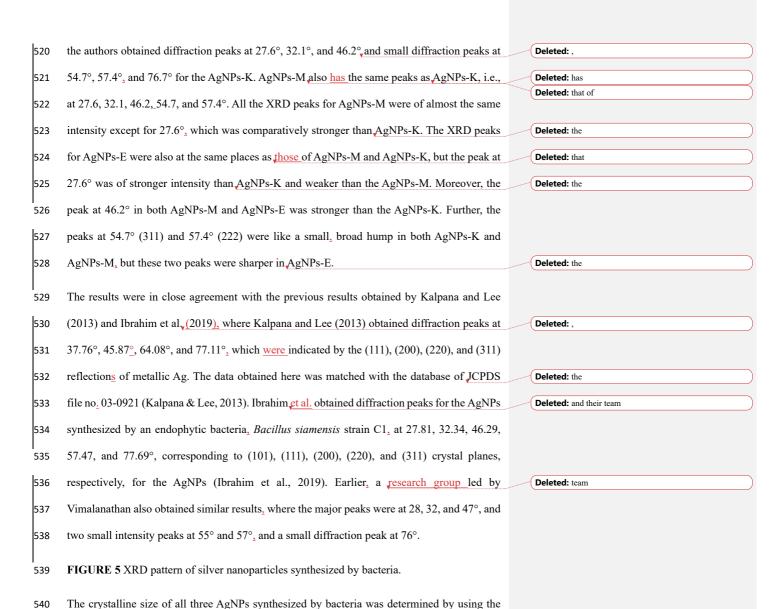
Commented [GR4]: ...his research group

Deleted:

Deleted: earlier also reported by Ibrahim and their team

Deleted: e

487	$1096.92~\text{cm}^{-1}\text{was}$ attributed to the (C-O) stretching of alcohols and esters, carboxylic acids,		
488	and C-N stretching of aliphatic amines (Saleh & Khoman Alwan, 2020). Based on the above		
489	information, it was further concluded that the presence of protein in the supernatant acts as a		
490	stabilizing and capping agent for stabilization, which binds to the synthesized AgNPs through		
491	free cysteine or amine groups in proteins (Saleh & Khoman Alwan, 2020). Previously, Kalpana		
492	and Lee (2013) also obtained bands for the AgNPs synthesized by using a culture of simulated		
493	microgravity-grown K. pneumoniae. The investigators obtained major intensity bands at		
 494	$2964.55~\text{cm}^{-1},~1262.22~\text{cm}^{-1},~1095.89~\text{cm}^{-1},~1021.96~\text{cm}^{-1},~800.73~\text{cm}^{-1},~\text{and small intensity}$		
495	bands at 2960.64 cm^{-1} , 1650.01 cm^{-1} , 865.33 cm^{-1} , 701 cm^{-1} -and 477.07 cm^{-1} .		
496	FIGURE 4 FTIR spectra of AgNPs synthesized by bacteria.		
1407	In the current investigation, authors have also obtained bands for the K. pneumoniae		Deleted: also
497			Deleted: also
498	synthesized AgNPs at 599, 963, 1229, 1693, 2891, and 3780 cm ⁻¹ which correspond to the		Deleted: s
499	bands obtained by Kalpana and Lee (Kalpana & Lee, 2013). Research group led by Peiris also	(Deleted: 2013
500	obtained four prominent FTIR bands at 1643, 1586, 1397, and 1042 cm ⁻¹ and concluded that		Deleted: A Deleted: team
501	the AgNPs synthesized by bacteria have enhanced stability because of the coating of AgNPs	(Deleted. tcam
502	by bacterial and media components (Peiris et al., 2018). AgNPs-M, and AgNPs-E displayed	(Deleted: .
503	similar bands as those of AgNPs-K with slight variation in their intensity.	(Deleted: that
303			Science. man
504	4.4. Phase identification of silver nanoparticles by XRD		
505	The XRD investigation was carried out to identify the crystalline phase of the AgNPs. A typical		
506	XRD pattern of all the bacterially synthesized AgNPs is shown in Figure 5. All the AgNPs		
507	exhibit three characteristic peaks of silver NPs at 27.6°, 32.1°, and 46.2°, and three small		
508	intensity peaks at 54.7°, 57.4°, and 76.7°. The major intensity peaks in all three types of		Deleted: and
509	bacterially synthesized AgNPs are at 32.1° followed by 46.2° and 27.6°. The XRD planes in		
510	all three types of AgNPs were 101, 111, 200, 220, and 311, as matched with the Joint		
511	Committee on Power Diffraction Standards (JCPDS) 03-0921. In the current investigations,		



Scherrer formula as given in Equation (2),

 $D = \frac{k\lambda}{\beta \cos \theta}$

(2)

541

542

554	Where,	
555	D =crystalline size,	
556	k = constant (0.9), and	
557	β = the FWHM values of the diffracted peaks.	
558	The highest intensity peak was used to find all the parameters in the Scherrer equation. The	Deleted: ¶
559	Gaussian peak fits were used to find the FWHM values and exact theta values. The calculated	
560	crystalline size was found to be around 16.88 nm, 18.00 nm, and 16.44 nm for AgNPs-K,	
561	AgNPs-M, and AgNPs-E. Therefore, it is well examined that the synthesized AgNPs showed a	
562	crystalline nature and 16.88 nm, 18.00 nm, and 16.44 nm crystallite sizes.	
563	4.5. Morphological analysis of silver nanoparticles by FESEM and elemental analysis by	
564	EDS	
565	Figure 6a-6f shows FESEM micrographs of AgNPs synthesized by K. pneumoniae (AgNPs-	
566	K). Figures 6a&b show a porous flakes-like structure that is embedded with bright-colored	
567	AgNPs. Figure 6c&d clearly shows rhombohedral-shaped AgNPs, whose size varies from 22-	Deleted: is varying
568	66 nm. These two images clearly show that the AgNPs are embedded in porous, sheet-like	
569	structures. Figure 6e&f show aggregated spherical-shaped structures. Previously, several	
570	investigators have shown similar morphology for the bacterially synthesized AgNPs.	
571	Figure 6g shows the EDS spot of the AgNPs-K ₂ while Figure 6h exhibits the EDS spectra and	
572	elemental table of the AgNPs-K. The EDS spectra in Figure 6h show peaks for Ag, Cl, Na, P,	Deleted: s
573	S, C, O, and N. Among these, the elements contributing the most to the sample were Ag (37.8%	Deleted: highest
574	At wt.), Cl (29.8%), and P and S were 0.4% each. The P and S were not present in trace amounts	Deleted: ;
575	in the AgNPs-K. The major impurities in the synthesized AgNPs-K are NaCl, which alone	
576	comprises 50%, which is due to the improper washing of the samples. Moreover, these two	
577	may also come from the nutrient broth used for growing the bacteria. While the presence of C,	

583	S, and P indicates the association of biomolecules with the synthesized AgNPs-K. Earlier.	
584	Sayyid and Zghair (2021) reported cube-shaped to irregular heterogeneous forms of AgNPs	
585	synthesized by K. pneumoniae, whose average size was 40.47 nm (Sayyid & Zghair, 2021).	Formatted: Font: Not Italic
586	Moreover, investigators further observed that the morphology by TEM was a pseudo-spherical	
587	shape of size 40-80 nm.	
588	FIGURE 6 FESEM images (a-f), EDS spot (g), and EDS spectra and elemental table (h) for	
589	AgNPs-K. FESEM images (i-1), EDS spot (m) and EDS spectra, and elemental table (n) for	
590	AgNPs-M. FESEM images (o-r), EDS spot (s) and EDS spectra, and elemental table (t) for	
591	AgNPs-E.	
592	Saleh and Alwan (2020) obtained spherical-shaped particles of size 26.84 to 44.42 nm. which	
593	were highly aggregated. Further, the investigators concluded that the conglomeration of the	
594	AgNPs occurs during the drying process (Saleh & Khoman Alwan, 2020).	Deleted: is
595	A research group led by Rasheed obtained nano-rod-like AgNPs of size 100-200 nm from the	Deleted: team
596	Conocarpus erectus plant, while oval-shaped AgNPs of size 110-150 nm were synthesized	
597	from Pseudomonas sps, and by applying the chemical reduction method, flower-like AgNPs	
598	of size 100-200 nm were obtained. So, the smallest size was reported from <i>Pseudomonas sps</i> ,	Deleted: was
599	which was oval-shaped.	
600	Figure 6i-l shows FESEM micrographs of AgNPs synthesized by the M. luteus (AgNPs-M).	
601	Figure 6i&j shows a high aggregation of the synthesized AgNPs-M. Figure 6k and Figure 6l	
602	show spherical-shaped AgNPs-M, whose size varies from 21-45 nm. Figure 6m shows the	Deleted: is varying
603	EDS spot of the AgNPs-M while Figure 6n exhibits the EDS spectra and elemental table of	
604	the AgNPs-M. The EDS spectra of AgNPs-M in Figure 6n show peaks for Ag, Cl, Na, P, S, C,	
605	O, and N. Out of all these, the major elements were mainly Ag (61% At wt.), Cl (21%), C	
606	(8.4%), N $(3.7%)$, and O $(2.6%)$. Other detected elements, such as Na, P, and S, were present	
ļ		

611	in trace amounts. The major impurity in the final sample was Cl _a which is due to improper	
612	washing of the sample. Moreover, it also came from the bacterial media i.e., nutrient broth.	
613	While the presence of C, N, S, and P indicates the presence of biomolecules with AgNPs-M.	Deleted: the
614	Figure 60-r shows FESEM micrographs of AgNPs synthesized by <i>E. aerogenes</i> (AgNPs-E).	
615	Figure 60&p shows a porous flakes-like structure that is embedded with the bright color of	
616	AgNPs. Figure 6q&r clearly shows rhombohedral-shaped AgNPs-E, whose size <u>varies</u> from	Deleted: is varying
617	24-60. The images clearly show that the AgNPs-E are embedded in the porous flakes-like	
618	structures. The particles are showing high aggregation, as evident from the SEM micrographs.	
619	Figure 6s shows the EDS spot of the AgNPs-E, while Figure 6t exhibits the EDS spectra and	
620	elemental table of the AgNPs-E. Figure 6t shows the spectra of Ag, Cl, Na, P, S, C, O, and N.	
621	Out of all these, the major elements were mainly Ag (52.1% At wt.), Cl (21.7%), C (9.8 %), O	Deleted: and
622	(8.2%), Na (4.0%), and N (3.1%). In addition to this, P and S were present in trace amounts,	
623	whose total composition was near 1.1%. The major impurities in the synthesized AgNPs-E are	
624	NaCl ₂ which alone comprises 25.7% ₂ which indicates the improper washing of the sample.	
625	Moreover, these two may also come from the nutrient broth used for growing the bacteria. The	
626	presence of C, S, N, and P indicates the association of enzymes and proteins from the E.	
627	aerogenes with the synthesized AgNPs-E. Table 1 shows the major elements present in all three	Deleted: with
628	types of AgNPs synthesized by bacteria.	
629	TABLE 1 Comparison between all the elements present in all three types of AgNPs.	
630	From the EDS data of all three types of AgNPs, it was found that Ag was present in the highest	
631	percentage in AgNPs-M and at least 37.8% in AgNPs-K. Among all the three types of AgNPs,	Deleted: while
632	Cl was present most in AgNPs-K and least in AgNPs-M (21.0%). The oxygen was present in	Deleted: maximum
633	the highest amount in AgNPs-E and the least in AgNPs-K, i.e., 8.2% and 2.8%, respectively.	Deleted: while
634	The carbon was highest in AgNPs-E (9.8%) and least 7.0% in AgNPs-K. Out of all the three	

642	types of AgNPs, Na was highest in AgNPs-K (21.8%) and least in AgNPs-M (0.4%). Among			
643	all the three samples of AgNPs, N was present highest in AgNPs-M (3.7%) and 3.1% in AgNPs-M (3.7%) an			
644	E, and it was not detected in AgNPs-K. The P and S were present almost identically in all the		Deleted: similar	
645	samples but least in AgNPs-K, i.e., 0.4%.			
646	In the current investigation, the authors <u>found</u> a broad peak of silver ions at 3 keV in all three		Deleted: have got	
647	types of AgNPs, which confirmed the reduction of Ag ⁺ to Ag ⁰ . Moreover, here the authors have		•	
ı	mainly, peaks in EDS for Ag, Cl, and carbon. The peaks for Ag, Cl, and S were consistent with	ال.	Deleted: got	
648			Deletea: got	$\frac{1}{2}$
649	the results obtained for the AgNPs synthesized by endophytic bacteria by Ibrahim and his team.		Deleted: their	
650	Ibrahim and his research group also concluded that the broad peak of silver ions was formed at		Deleted: their team	
651	3 keV, which indicated the reduction of Ag^{2+} to Ag^0 (Ibrahim et al., 2019).			
CE2	Table 2 shows the major microbial proteins and enzymes present in <i>K. pneumoniae, M. luteus</i> ,			
652				
653	and E. aerogenes, while Table 3 shows the comparative analysis of all the previously reported		Formatted: Font: Not Italic)
654	bacterially synthesized AgNPs with the current investigation.			
655	TABLE 2 The major microbial proteins and enzymes present in K. pneumoniae, M. luteus,			
656	and E. aerogenes.			
657	TABLE 3 The comparative analysis of all the previous studies and current investigations			
658	of the bacterially synthesized AgNPs.			
659	From all the previous investigations, it was revealed that the largest size of AgNPs was			
660	40.47±89 nm synthesized by using K. pneumoniae, whose shape was cube to spherical. The		Formatted: Font: Not Italic	
661	smallest AgNPs were synthesized by <i>B. cereus</i> , whose size was 2-16 nm and spherical shaped.		Formatted: Font: Not Italic	
662	In the current investigation, the size of the synthesized AgNPs varied from 21 nm to 66 nm.			
663	Earlier, three more investigators synthesized AgNPs from different species of K. pneumoniae		Deleted: Klebsiella	
664	which were mainly spherical shaped and cube-shaped. Except in one or two cases, most of the	(Formatted: Font: Not Italic	
665	synthesized AgNPs were spherical in shape, whereas in two cases, cube shaped AgNPs were			

obtained. In terms of elemental composition and purity, AgNPs synthesized by B. siamensis 672 strain C1 were purest, where Ag was 91.8% while the remaining was impurity mainly by Cl 673 and S, whereas in our case the Ag percentage varied from 37.8% to 61.6%, i.e., less than the 674 earlier reported by Ibrahim and his team (Ibrahim et al., 2021). The lower purity could be due 675 Deleted: their to improper washing of the AgNPs during centrifugation. From the UV-Vis study, it was found 676 that the absorbance peak of AgNPs synthesized from different bacteria could be varied from 677 678 400 to 510 nm based on the size and shape of the synthesized AgNPs. From XRD and FTIR, it 679 was found that the majority of the peaks and bands remain the same in all the syntheses with 680 slight variations, respectively. 681 4.6. Batch adsorption study of methyl orange dye by AgNPs 682 MO dye shows the highest absorbance at 464 nm when examined using a UV-Vis spectrophotometer. The AgNPs-M, AgNPs-K, and AgNPs-E treated MO were measured for 683 684 their color intensity in an aqueous dye solution for up to 120 minutes at a regular interval of 30 Deleted: a time of minutes. With passing time, the concentration of MO dye in the sample decreased gradually. 685 which is evident from the UV-visible spectra (Figure 7 a, b, and c). So, the maximum removal 686 687 of MO dye was found after 120 minutes using AgNPs-M. The readings at an interval of every 688 30 minutes show a slow decrease in the concentration and absorbance of the dye; hence, the Deleted: 689 decrease in the graph can be observed easily as it moves from 0 minutes to 120 minutes. Figure 690 7 a, b, and c shows the MO dye absorbance by UV-Vis spectroscopy at different time intervals. FIGURE 7 MO dye removal by different types of AgNPs with respect to contact time as 691 measured by UV-Vis spectrophotometer: a) AgNPs-K, b) AgNPs-M, and c) AgNPs-E. 692 4.7. Percentage removal of MR dye by all the AgNPs 693 AgNPs-M removed MO dye 2.34% at 30 minutes, 4.37% at 60 minutes, 14.83% at 90 minutes, 694 695 and 19.24% at 120 minutes. AgNPs-K removed MO dyeat 1.5% at 30 minutes, 4.06% at 60

minutes, 9.56% at 90 minutes, and 15.03% at 120 minutes. AgNPs-E removes MO dye 1.52% 699 at 30 minutes, 2.36% at 60 minutes, 3.86% at 90 minutes, and 4.15% at 120 minutes. By 700 Deleted: minutes. 701 comparing all the AgNPs mentioned above, we can observe that AgNP-M has the highest Deleted: more efficiency of dye removal and AgNPs-E has the <u>lowest</u> efficiency of dye removal. Figure 8 702 Deleted: least shows the percentage removal of MO dye by all three types of AgNPs. 703 FIGURE 8 Percentage removal of MO dye by all three types of AgNPs. 704 705 Earlier, Gola and their colleagues successfully utilized AgNPs, synthesized by Aspergillus sps., Commented [GR5]:his colleagues Formatted: Font: Italic 706 to degrade the reactive yellow dye in an aqueous solution through photocatalysis, Here the Deleted: Earlier Gola and their team photocatalytically degraded the reactive yellow dye from the aqueous solution by using AgNPs synthesized by *Aspergillus sps*. initial dye concentration was about 20-100 mg/L, where about 1 g/L of retentate biomass of the 707 708 fungus removed 82-100% dye, respectively. As the initial dye concentration increased the Deleted: was decolorization efficiency of the biomass retentate decreased from 9.2% to 32.3% (Gola et al., Deleted: was 709 2021). Rasheed and his research group removed reactive black 5 (RB5), methylene blue (MB), 710 Deleted: their Deleted: team 711 4-nitrophenol (4-NP), and reactive red 120 dye (RR120) from the aqueous solutions by using Deleted: . AgNPs synthesized from C. erectus (plant), Pseudomonas sps, and the chemical reduction 712 method. The removal of MB and 4-NP was investigated along with the absence and presence 713 714 of AgNPs (catalysts) and variable doses of a reducing agent (NaBH₄). The removal of RB5 and 715 RR120 dye was carried out in the absence of a reducing agent and variable doses of AgNPs. 716 The bacterially synthesized AgNPs showed almost 100% removal of MB dye within 30 717 minutes, while AgNPs synthesized by the chemical reduction method showed almost 93.2% removal of RR120, whose more detailed outcomes are compared in Table 4 (Rasheed et al., 718 2023). Previously, a research group led by Batool synthesized AgNPs from Salvinia molesta Deleted: team 719 720 and used them for the removal of methylene blue dye from the aqueous solution. Where, the Deleted: Deleted: where 721 highest adsorption capacity of the dye on the surface of AgNPs was 121.04 mg/g by the Commented [GR6]: Sentence formation 722 Langmuir isotherm (Batool, Daoush & Hussain, 2022). Bhankhar et al. removed MO up to Deleted: and their group 83% by using chemically synthesized AgNPs in the presence of NaBH4 under optimized 723

conditions (Bhankhar et al., 2014). Table 4 depicts the summarized form of all the 739 investigations and current investigations where AgNPs were used for the removal of MO from 740 wastewater. 741 TABLE 4 Summarized form of all the investigations and current investigations where 742 AgNPs were used for the removal of various dyes from wastewater. 743 744 From all the above investigations mentioned in Table 4, it was concluded that previously only one attempt was made to remove MO dye that too by using AgNPs synthesized by chemical 745 reduction method, where the removal percentage was 83% within 2 minutes (Bhankhar et al., 746 2014). Most of the investigators tried to remove MB dye by using AgNPs synthesized from 747 plants and bacteria by chemical method. There was only one attempt where dyes (MB, 4-NP, Deleted: 748 749 RB5, and RR120) were removed by using AgNPs synthesized by Pseudomonas sps, where the removal efficiency varied from 40-100% under optimized conditions. The highest MB removal 750 751 was observed with AgNPs synthesized from Pseudomonas sps. in comparison to the AgNPs synthesized from C. erectus (100-200 nm) and chemical reduction method (100-200 nm), 752 which could be attributed to the smallest average size (110-150 nm) of the Pseudomonas sps 753 754 mediated synthesized AgNPs (Rasheed et al., 2023). Moreover, in current investigation, Deleted: Deleted: our AgNPs-M have the smallest average size (21-45 nm), which exhibited the highest MO dye 755 756 removal, i.e., 19.24% in 2 hours. In our current investigation, the removal percentage of MO Deleted: i.e. 757 was just 4-19.24% which is almost 5 to 15 folds less than the attempt by using AgNPs 758 synthesized by the chemical method. This could be so because, in the current investigation, the dose of the AgNPs was 1 mg/100 mL whereas Rasheed et al used 100 mg/50 mL of AgNPs 759 760 synthesized from Pseudomonas sps for the removal of RB5 and RR120 for the removal of MB₂ 761 and 4-NP dye (20 mg AgNPs) was used. Zaman and their research team successfully achieved Commented [GR7]: ...his **Deleted:** The study by Zaman and their group photocatalytically degraded 94% MB from the aqueous 762 a 94% degradation of MB in an aqueous solution using photocatalysis under solar irradiation, solution under solar irradiation (Zaman et al., 2023). 763

To achieve a higher removal efficiency of dye, higher dose of AgNPs is suggested. Moreover, 771 further improvement in the dye removal by AgNPs could be done by using different types of 772 773 chemical reducing agents (NaBH₄) along with the AgNPs (Rasheed et al., 2023). However, the Deleted: chemical utilization of higher doses of AgNPs for the removal of dye at a commercial level from 774 wastewater is economically feasible. From the investigation, it was also concluded that the 775 morphology of the AgNPs also affects the removal efficiency of the dyes, i.e., smaller particles 776 Deleted: i.e. 777 have a high removal efficiency (Zaman et al., 2023), as evident from the current investigation 778 and study done by Rasheed et al. So, to achieve higher efficiency of dye removal, it is advisable Deleted: and their group to synthesize controlled (small size) and uniform AgNPs. Moreover, the removal of dyes under 779 780 irradiation (solar, UV, etc.) may increase the removal efficiency using photocatalytic Deleted: s 781 degradation. In addition to this, pH and temperature can be optimized to obtain a higher Deleted: , Deleted: from 782 percentage of dye removal by using bacterially synthesized MO dye in the aqueous solutions. 783 4.8. Evaluation of the antimicrobial activity of the synthesized AgNPs AgNPs-K shows a ZOI of 11 mm against B. megaterium and E. fecalis. B. subtilis shows a 784 moderate ZOI of 10 mm when compared with other zones, and B. cereus shows a 9 mm ZOI 785 786 due to the effect of AgNPs. Deleted: Earlier, Syyaid and Zghair (2021) also used the K. pneumoniae synthesized AgNPs for their 787 788 antimicrobial activity against S. aureus and E. coli. The investigators used about 40-50 µg/mL of AgNPs and found that E. coli was more susceptible to AgNPs compared to Gram-positive 789 bacteria such as S. aureus. Further, the investigators suggested that this could be due to 790 variations in the thickness and composition of their cell walls, like peptidoglycan (Sayyid & 791 Zghair, 2021). Saleh and Alwanz (2020) assessed the three concentrations of AgNPs (50, 10, 792 and 150 µg/mL) synthesized from K. pneumoniae and evaluated them against E. coli, P. 793 aeruginosa, S. aureus, and B. cereus. Investigators reported that the highest concentration, i.e., 794

802	150 μg/mL, was found to be most effective against these pathogens in comparison to 50 and	Deleted: the
803	$100~\mu\text{g/mL}$. This suggests that the increase in the concentration of AgNPs increases the	
804	antibacterial activity (Saleh & Khoman Alwan, 2020).	
805	The use of AgNPs-M for antibacterial activity (Gnanamoorthy et al., 2022) using different	
806	bacteria like B. subtilis, B. cereus, B. megaterium, and E. fecalis shows different ZOI. AgNPs-	Formatted: Font: Not Italic
807	M shows a maximum ZOI of 12 mm against B. megaterium and a minimum ZOI against B.	
808	cereus of 8 mm. It shows a moderate ZOI of 9 mm against E. fecalis and 11 mm against B.	
809	subtilis, B. megaterium was more susceptible than E. fecalis, and B. subtilis was moderately	Deleted: The
040		Formatted: Font: Not Bold
810	susceptible, and B. cereus was less susceptible to AgNPs-M. B. cereus gives a greater ZOI of	Formatted: Font: Not Italic
811	11 mm due to the effect of AgNPs-E. The lowest ZOI is observed against B. megaterium, which	Deleted: the
812	is 8 mm and also shows a 10 mm, ZOI by B. subtilis and E. fecalis.	Deleted: the
012	is 6 min and also shows a 10 min. 201 by D. subtits and E. Jecaus.	
813	Previously, a research group led by Gola obtained a ZOI of about 13 and 10 mm against E. coli	Deleted: team
814	and S. aureus, respectively, for the AgNPs synthesized by Aspergillus sps. Further, the	
815	investigator evaluated the synergistic effect of AgNPs and penicillin against E. coli and S.	
816	aureus and showed 0.49- and 0.36-fold increases in the ZOI ₂ respectively ₂ in comparison to the	
817	AgNPs and penicillin alone (Gola et al., 2021).	
818	Pagently, Hag and Alter (2021) synthesized anystalling enhanced should 12.27 nm sized	
010	Recently, Haq and Akter (2021) synthesized crystalline, spherical-shaped, 13-27 nm sized	
819	AgNPs by using Paenarthrobacter nicotinovorans MAHUQ-43. Further, it was evaluated as	Deleted: ,
820	an antibacterial agent against B. cereus ATCC 10876 and P. aeruginosa ATCC 10145, where	
821	the MIC and MBC for both pathogens were 12.5 $\mu g/mL$ and 25 $\mu g/mL$, respectively. The ZOI	
822	at 30 μL against <i>P. aeruginosa</i> was 15.5±0.8 mm and 13.6±0.5 mm against <i>B. subtilis</i> whereas	Formatted: Font: Not Italic
823	at 60 μL the ZOI against <i>P. aeruginosa</i> was 24.7±0.9 mm and against <i>B. subtilis</i> it was 19.3±1.0	Deleted:
824	mm (Huq & Akter, 2021).	Formatted: Font: (Default) Times New Roman, 12 pt

832	A research group led by Ibrahim synthesized spherical-shaped AgNPs of size 5-7.06 nm by Deleted: team
833	using B. cereus, whose antimicrobial activity was evaluated against a group of five different
834	bacterial strains, namely: Staphylococcus epidermidis, S. aureus, E. coli, Salmonella enterica,
835	and Porteus mirabilis, by the agar-disc diffusion method, whose ZOI was 32.12 ± 0.55, 38.25 Formatted: Font: Not Bold
836	$\pm 0.05, 33.05 \pm 1.33, 30.73 \pm 0.25,$ and 35.44 ± 1.08 mm at a concentration of about 200 µg/mL
837	of AgNPs (Ibrahim et al., 2021). Figure 9 shows the antibacterial activity of Petri plates of the
838	AgNPs against tested bacterial species. Table 5 shows a comparison of the antibacterial activity
839	of the current investigation with previously reported studies.
840	FIGURE 9 Antibacterial activity, zone of inhibition of AgNPs synthesized against the tested
841	bacterial species.
842	TABLE 5 Summarized form of comparison of antibacterial activity of AgNPs of earlier
843	reported work and current investigation.
844	The difference between the antibacterial effect against GPB and GNB bacteria over here might
845	be due to the morphological differences in both types of bacteria (Jubeh, Breijyeh & Karaman,
846	2020). GPB has a thick peptidoglycan layer, while GNB has a thin peptidoglycan layer but a Deleted: have
847	thick lipopolysaccharide layer (Pasquina-Lemonche et al., 2020). A similar reason was also
848	given by several other investigators for the antimicrobial activity of the synthesized AgNPs
849	(Kalpana & Lee, 2013). Investigators reported that spherical AgNPs have higher
850	antibacterial/antimicrobial activity due to their high SVR (Al-Ogaidi & Rasheed, 2022).
851	Moreover, due to their large surface area, they could bind with various ligands. AgNPs can
852	easily infiltrate the bacterial cell membrane, and that is the reason for their enhanced
853	antimicrobial activity, which might improve more with a further decrease in the size of AgNPs
854	(Anees Ahmad et al., 2020; Wypij et al., 2021). AgNPs get attached to the cell membrane.
855	where they release Ag ions slowly. Further, AgNPs are reported to develop pits in the cell wall
1	

of microorganisms_a which leads to enhanced permeability and leakage of cellular components through the plasma membrane (Tripathi et al., 2017; Matras et al., 2022).

5. Conclusions

859 860

861

862

863

864 865

866

867

868 869

870

871

872

873

874

875

876

877

878

879

880

881

882

883

The shape and method of synthesis of silver nanoparticles can affect their antimicrobial properties. The current study aimed to produce biocompatible and morphologically consistent silver nanoparticles using an environmentally friendly method. Microbial species possess a range of enzymes, such as reductase, that convert metallic silver ions into silver nanoparticles, which is facilitated by bacterial molecules, which act as both capping and reducing agents. In this study, spherical, oval, and porous sheet shapes of silver nanoparticles were successfully synthesized by using different bacterial strains via the green route using a minimal amount of chemicals. The AgNPs synthesised exhibited UV-Vis absorbance maxima at wavelengths of 475 nm, 428 nm, and 503 nm. The XRD analysis revealed the presence of well-defined crystal structures in the synthesised silver nanoparticles (AgNPs), with distinct peaks observed at 26.2°, 32.1°, and 47.2°. Meanwhile, the FTIR analysis detected characteristic bands at 599 cm⁻¹, 963 cm⁻¹, 1693 cm⁻¹, 2299 cm⁻¹, 2891 cm⁻¹, and 3780 cm⁻¹ for all types of AgNPs. AgNPs range in size from 10 nm to several microns, with shapes ranging from spherical to porous sheets, whereas, percentage of Ag varied from 37.8% (wt.%) to 61.6%. The AgNPs synthesised by Micrococcus luteus exhibited the highest percentage of methyl orange dye removal, reaching up to 20%, and also exhibited maximum antimicrobial activity against B. megaterium, measuring 12 mm. The higher dye removal efficiency and antimicrobial activity of AgNPs-M could be due to the smallest size of the AgNPs produced by M. luteus. Therefore, shape significantly influences the ability to remove dyes and antimicrobial properties. Such bacterial-based green synthesis of AgNPs acts as a potential and sustainable approach for material synthesis. Moreover, such approaches could be highly valuable in the field of biomedicine.

Funding: This research was funded by the Deanship of Scientific Research at King Khalid University under the grant number R.G.P. 2/174/44.

Commented [GR8]: Font type inconsistent

Deleted: The silver nanoparticles have antimicrobial potential, which could be further affected by their morphology and route of synthesis. Chemically, it is possible to control the morphology and uniformity of the synthesized silver nanoparticles, but while using it for antimicrobial activities biocompatibility is a major issue. So, bacterialmediated synthesis of silver nanoparticles could solve the biocompatibility issue by maintaining the uniformity and size of the nanoparticles. The present research was conducted to obtain biocompatible and morphologically uniform types of silver nanoparticles by an eco-friendly route. The microbial have various enzymes like reductas which reduces the metallic silver ion into silver nanoparticles by using bacterial molecules as a capping and reducing agent. So, here the authors have successfully synthesized, biocompatible, uniform 21-66 nm sized silver nanoparticles of spherical, oval, and porous sheet type by using the least chemicals. The microscopic techniques confirm the spherical shape of AgNPs, while EDS shows the purity of the AgNPs. The XRD exhibited the crystalline nature of the AgNPs, while FTIR showed the typical IR bands for the AgNPs. FTIR also showed the presence of organic biomolecules with the synthesized AgNPs. The methyl orange dye removal percentage for the AgNPs was highest up to 20% with the smallest AgNPs synthesized by Micrococcus luteus. The highest antibacterial activity was exhibited with AgNPs-M against B. megaterium i.e., 12 mm which could also be attributed to the smaller size of the AgNPs synthesised by M. luteus. So, morphology plays an important role in dye removal capacity and antimicrobial activity.

- 915 Acknowledgements: The authors extend their appreciation to the Deanship of Scientific
- 916 Research at King Khalid University for supporting this research work. The authors are also
- 917 thankful to Department of Life Sciences, Hemchandracharya North Gujarat University for
- 918 providing the lab facilities.
- 919 References
- 920 Adibah N, Firdianti BE, Suprapto S. 2023. Synthesis of Silver Nanoparticles Using Response
- 921 Surface Methodology. Journal of Nano- and Electronic Physics 15. DOI:
- 922 10.21272/jnep.15(3).03001.
- 923 Al-Ogaidi MAZ, Rasheed BG. 2022. Enhancement of Antimicrobial Activity of Silver
- 924 Nanoparticles Using Lasers. Lasers in Manufacturing and Materials Processing 9:610-
- 925 621. DOI: 10.1007/s40516-022-00192-4.
- 926 Al-Tohamy R, Ali SS, Li F, Okasha KM, Mahmoud YA-G, Elsamahy T, Jiao H, Fu Y, Sun J.
- 927 2022. A critical review on the treatment of dye-containing wastewater: Ecotoxicological
- and health concerns of textile dyes and possible remediation approaches for environmental
- 929 safety. Ecotoxicology and Environmental Safety 231:113160. DOI:
- 930 https://doi.org/10.1016/j.ecoenv.2021.113160.
- 931 Anees Ahmad S, Sachi Das S, Khatoon A, Tahir Ansari M, Afzal Mohd, Saquib Hasnain M,
- 932 Kumar Nayak A. 2020. Bactericidal activity of silver nanoparticles: A mechanistic review.
- 933 Materials Science for Energy Technologies 3:756–769. DOI:
- 934 https://doi.org/10.1016/j.mset.2020.09.002.
- 935 Austin W, Granger S, Felicia R, P PL, E FD, G FV, T TJ. 2020. Newly Named Klebsiella
- 936 aerogenes (formerly Enterobacter aerogenes) Is Associated with Poor Clinical Outcomes
- 937 Relative to Other Enterobacter Species in Patients with Bloodstream Infection. *Journal of*
- 938 *Clinical Microbiology* 58:10.1128/jcm.00582-20. DOI: 10.1128/jcm.00582-20.

- 939 Ballén V, Gabasa Y, Ratia C, Ortega R, Tejero M, Soto S. 2021. Antibiotic Resistance and
- 940 Virulence Profiles of Klebsiella pneumoniae Strains Isolated From Different Clinical
- 941 Sources. Frontiers in Cellular and Infection Microbiology 11.
- 942 Batool M, Daoush WM, Hussain MK. 2022. Dye Sequestration Using Biosynthesized Silver
- 943 Nanoparticles Adsorbent in Aqueous Solutions. Crystals 12. DOI:
- 944 10.3390/cryst12050662.
- 945 Betts HD, Whitehead C, Harris HH. 2021. Silver in biology and medicine: opportunities for
- metallomics researchers. *Metallomics* 13:mfaa001. DOI: 10.1093/mtomcs/mfaa001.
- 947 Bhankhar A, Giri M, Yadav K, Jaggi N. 2014. Study on degradation of methyl orange-an azo
- 948 dye by silver nanoparticles using UV-Visible spectroscopy. Indian Journal of Physics
- 949 88:1191–1196. DOI: 10.1007/s12648-014-0555-x.
- 950 Bouafia A, Laouini SE, Ahmed ASA, Soldatov A V., Algarni H, Chong KF, Ali GAM. 2021.
- The recent progress on silver nanoparticles: Synthesis and electronic applications.
- 952 Nanomaterials 11. DOI: 10.3390/nano11092318.
- 953 Carter EL, Boer JL, Farrugia MA, Flugga N, Towns CL, Hausinger RP. 2011. Function of UreB
- in Klebsiella aerogenes Urease. Biochemistry 50:9296–9308. DOI: 10.1021/bi2011064.
- 955 Cekuolyte K, Gudiukaite R, Klimkevicius V, Mazrimaite V, Maneikis A, Lastauskiene E. 2023.
- 956 Biosynthesis of Silver Nanoparticles Produced Using Geobacillus spp. Bacteria.
- 957 Nanomaterials 13. DOI: 10.3390/nano13040702.
- 958 Chen D, Wang Q, Li Y, Li Y, Zhou H, Fan Y. 2020. A general linear free energy relationship for
- predicting partition coefficients of neutral organic compounds. *Chemosphere* 247:125869.
- 960 DOI: https://doi.org/10.1016/j.chemosphere.2020.125869.

V. 2023. Phytonanofabrication of Copper Oxide by Albizia saman and Their Potential as 962 an Antimicrobial Agent and Remediation of Congo Red Dye from Wastewater. Water 963 15:3787. DOI: 10.3390/w15213787. 964 Cui G, Bai Y, Li W, Gao Z, Chen S, Qiu N, Satoh T, Kakuchi T, Duan Q. 2017. Synthesis and 965 characterization of Eu(III) complexes of modified d-glucosamine and poly(N-966 isopropylacrylamide). Materials Science and Engineering: C 78:603-608. DOI: 967 https://doi.org/10.1016/j.msec.2017.03.059. 968 Das A, Mishra S. 2017. Removal of textile dye reactive green-19 using bacterial consortium: 969 970 Process optimization using response surface methodology and kinetics study. Journal of 5:612-627. DOI: Environmental Chemical Engineering 971 https://doi.org/10.1016/j.jece.2016.10.005. 972 Dash S, Chaudhuri H, Gupta R, Nair UG. 2018. Adsorption study of modified coal fly ash with 973 sulfonic acid as a potential adsorbent for the removal of toxic reactive dyes from aqueous 974 solution: Kinetics and thermodynamics. Journal of Environmental Chemical Engineering 975 6:5897–5905. DOI: https://doi.org/10.1016/j.jece.2018.05.017. 976 Degefa A, Bekele B, Jule LT, Fikadu B, Ramaswamy S, Dwarampudi LP, Nagaprasad N, 977 978 Ramaswamy K. 2021. Green Synthesis, Characterization of Zinc Oxide Nanoparticles, and 979 Examination of Properties for Dye-Sensitive Solar Cells Using Various Vegetable Extracts. Journal of Nanomaterials 2021. DOI: 10.1155/2021/3941923. 980 El-Khatib AM, Badawi MS, Ghatass ZF, Mohamed MM, Elkhatib M. 2018. Synthesize of 981 Silver Nanoparticles by Arc Discharge Method Using Two Different Rotational Electrode 982 Shapes. Journal of Cluster Science 29:1169-1175. DOI: 10.1007/s10876-018-1430-2. 983

Choudhary N, Chaudhari J, Mochi V, Patel P, Ali D, Alarifi S, Sahoo DK, Patel A, Kumar Yadav

961

984	Esmail R, Afshar A, Morteza M, Abolfazl A, Akhondi E. 2022. Synthesis of silver nanoparticles
985	with high efficiency and stability by culture supernatant of Bacillus ROM6 isolated from
986	Zarshouran gold mine and evaluating its antibacterial effects. BMC Microbiology 22. DOI:
987	10.1186/s12866-022-02490-5.
988	Giri AK, Jena B, Biswal B, Pradhan AK, Arakha M, Acharya S, Acharya L. 2022. Green
989	$synthesis\ and\ characterization\ of\ silver\ nanoparticles\ using\ Eugenia\ roxburghii\ DC.\ extract$
990	and activity against biofilm-producing bacteria. Scientific Reports 12:8383. DOI:
991	10.1038/s41598-022-12484-y.
992	Gnanamoorthy G, Kumar Yadav V, Ali D, Ramar K, Gokhlesh Kumar, Narayanan V. 2022. New
993	designing (NH4)2SiP4O13 nanowires and effective photocatalytic degradation of
994	Malachite green and antimicrobial properties. Chemical Physics Letters 803:139817. DOI:
995	https://doi.org/10.1016/j.cplett.2022.139817.
996	Gola D, Tyagi PK, Arya A, Gupta D, Raghav J, Kaushik A, Agarwal M, Chauhan N, Srivastava
997	SK. 2021. Antimicrobial and dye degradation application of fungi-assisted silver
998	nanoparticles and utilization of fungal retentate biomass for dye removal. Water
999	Environment Research 93:2727–2739. DOI: https://doi.org/10.1002/wer.1629.
1000	Gupta N, Yadav VK, Gacem A, Al-Dossari M, Yadav KK, Abd El-Gawaad NS, Ben Khedher
1001	N, Choudhary N, Kumar P, Cavalu S. 2022. Deleterious Effect of Air Pollution on Human
1002	Microbial Community and Bacterial Flora: A Short Review. International Journal of
1003	Environmental Research and Public Health 19:15494. DOI: 10.3390/ijerph192315494.
1004	Gurunathan S. 2019. Rapid biological synthesis of silver nanoparticles and their enhanced
1005	antibacterial effects against Escherichia fergusonii and Streptococcus mutans. Arabian
1006	Journal of Chemistry 12:168–180. DOI: https://doi.org/10.1016/j.arabjc.2014.11.014.

1007	Hamouda RA, Hussein MH, Abo-elmagd RA, Bawazir SS. 2019. Synthesis and biological
1008	characterization of silver nanoparticles derived from the cyanobacterium Oscillatoria
1009	limnetica. Scientific Reports 9:13071. DOI: 10.1038/s41598-019-49444-y.
1010	Harja M, Buema G, Bucur D. 2022. Recent advances in removal of Congo Red dye by
1011	adsorption using an industrial waste. Scientific Reports 12:6087. DOI: 10.1038/s41598-
1012	022-10093-3.
1013	Horne J, De Bleye C, Lebrun P, Kemik K, Van Laethem T, Sacré P-Y, Hubert P, Hubert C,
1014	Ziemons E. 2023. Optimization of silver nanoparticles synthesis by chemical reduction to
1015	enhance SERS quantitative performances: Early characterization using the quality by
1016	design approach. Journal of Pharmaceutical and Biomedical Analysis 233:115475. DOI:
1017	https://doi.org/10.1016/j.jpba.2023.115475.
1018	Huq MA, Akter S. 2021. Bacterial mediated rapid and facile synthesis of silver nanoparticles
1019	and their antimicrobial efficacy against pathogenic microorganisms. Materials 14. DOI:
1020	10.3390/ma14102615.
1021	I TW, David A. 1972. Catalase Test as an Aid to the Identification of Enterobacteriaceae.
1022	Applied Microbiology 24:58–61. DOI: 10.1128/am.24.1.58-61.1972.
1023	Ibrahim S, Ahmad Z, Manzoor MZ, Mujahid M, Faheem Z, Adnan A. 2021. Optimization for
1024	biogenic microbial synthesis of silver nanoparticles through response surface
1025	methodology, characterization, their antimicrobial, antioxidant, and catalytic potential.
1026	Scientific Reports 11. DOI: 10.1038/s41598-020-80805-0.
1027	Ibrahim E, Fouad H, Zhang M, Zhang Y, Qiu W, Yan C, Li B, Mo J, Chen J. 2019. Biosynthesis
1028	of silver nanoparticles using endophytic bacteria and their role in inhibition of rice
1029	pathogenic bacteria and plant growth promotion. RSC Advances 9:29293-29299. DOI:

10.1039/c9ra04246f.

- 1031 Imoisili PE, Nwanna EC, Jen T-C. 2022. Facile Preparation and Characterization of Silica
- Nanoparticles from South Africa Fly Ash Using a Sol-Gel Hydrothermal Method.
- 1033 *Processes* 10:2440. DOI: 10.3390/pr10112440.
- 1034 Javaid A, Oloketuyi SF, Khan MM, Khan F. 2018. Diversity of Bacterial Synthesis of Silver
- Nanoparticles. *BioNanoScience* 8:43–59. DOI: 10.1007/s12668-017-0496-x.
- 1036 Jubeh B, Breijyeh Z, Karaman R. 2020. Resistance of gram-positive bacteria to current
- antibacterial agents and overcoming approaches. Molecules 25. DOI:
- 1038 10.3390/molecules25122888.
- 1039 Juma M (Wabwile), Nancy MM, Birech Z, Moraa Ondieki A, Maaza M, Mkhoztwa D. 2023.
- 1040 Using laser ablation in liquid (LASIS) method to synthesize silver nanoparticles for SERS
- 1041 applications. *Materials Today: Proceedings*. DOI:
- 1042 https://doi.org/10.1016/j.matpr.2023.07.372.
- 1043 Kalpana D, Lee YS. 2013. Synthesis and characterization of bactericidal silver nanoparticles
- using cultural filtrate of simulated microgravity grown Klebsiella pneumoniae. Enzyme
- and Microbial Technology 52:151–156. DOI: 10.1016/j.enzmictec.2012.12.006.
- 1046 Kalwar K, Shan D. 2018. Antimicrobial effect of silver nanoparticles (AgNPs) and their
- 1047 mechanism a mini review. Micro & Nano Letters 13:277-280. DOI:
- 1048 https://doi.org/10.1049/mnl.2017.0648.
- 1049 Karami-Zarandi M, Rahdar HA, Esmaeili H, Ranjbar R. 2023. Klebsiella pneumoniae: an
- update on antibiotic resistance mechanisms. Future Microbiology 18:65-81. DOI:
- 1051 10.2217/fmb-2022-0097.
- 1052 Karunakaran G, Jagathambal M, Gusev A, Torres JAL, Kolesnikov E, Kuznetsov D. 2017.
- 1053 Rapid Biosynthesis of AgNPs Using Soil Bacterium Azotobacter vinelandii With

1054	Promising Antioxidant and Antibacterial Activities for Biomedical Applications. JOM
1055	69:1206–1212. DOI: 10.1007/s11837-016-2175-8.
1056	Kumar N, Dubey RC. 2022. Biosynthesis of silver nanoparticles using the endophyte
1057	Enterobacter roggenkampii BLS02 from Barleria lupulina and their role in the inhibition
1058	of food borne bacteria. <i>Vegetos</i> . DOI: 10.1007/s42535-022-00514-z.
1059	Kyung JW, Cheong KH, Woo KK, Sook S, Hyun KS, Ho PY. 2008. Antibacterial Activity and
1060	Mechanism of Action of the Silver Ion in Staphylococcus aureus and Escherichia coli.
1061	Applied and Environmental Microbiology 74:2171–2178. DOI: 10.1128/AEM.02001-07.
1062	Lai Y, Zhu S, Li J, Zhang H, Qi T. 2023. One-step synthesis of micro-sized flake silver particles
1063	as electrically conductive adhesive fillers in printed electronics. Journal of Industrial and
1064	Engineering Chemistry 121:77–91. DOI: https://doi.org/10.1016/j.jiec.2023.01.008.
1065	Matras E, Gorczyca A, Przemieniecki SW, Oćwieja M. 2022. Surface properties-dependent
1066	antifungal activity of silver nanoparticles. Scientific Reports 12:18046. DOI:
1067	10.1038/s41598-022-22659-2.
1068	Merciecca T, Bornes S, Nakusi L, Theil S, Rendueles O, Forestier C, Miquel S. 2022. Role of
1069	Klebsiella pneumoniae Type VI secretion system (T6SS) in long-term gastrointestinal
1070	colonization. Scientific Reports 12:16968. DOI: 10.1038/s41598-022-21396-w.
1071	Modi S, Yadav VK, Amari A, Osman H, Igwegbe CA, Fulekar MH. 2023. Nanobioremediation:
1072	a bacterial consortium-zinc oxide nanoparticle-based approach for the removal of
1073	methylene blue dye from wastewater. Environmental Science and Pollution Research
1074	30:72641–72651. DOI: 10.1007/s11356-023-27507-y.
1075	Murukutti MK, Jena H. 2022. Synthesis of nano-crystalline zeolite-A and zeolite-X from Indian
1076	coal fly ash, its characterization and performance evaluation for the removal of Cs+ and

Sr2+ from simulated nuclear waste. Journal of Hazardous Materials 423:127085. DOI: 1077 https://doi.org/10.1016/j.jhazmat.2021.127085.1078 Naganthran A, Verasoundarapandian G, Khalid FE, Masarudin MJ, Zulkharnain A, Nawawi 1079 NM, Karim M, Abdullah CAC, Ahmad SA. 2022. Synthesis, Characterization and 1080 Biomedical Application DOI: 1081 of Silver Nanoparticles. Materials 15. 10.3390/ma15020427. 1082 1083 Nisha C, Bhawana P, Fulekar MH. 2017. Antimicrobial Potential of Green Synthesized Silver nanoparticles using Sida acuta Leaf extract. 1084 Pan S, Yao T, Du L, Wei Y. 2020. Site-saturation mutagenesis at amino acid 329 of Klebsiella 1085 pneumoniae halophilic α-amylase affects enzymatic properties. Journal of Bioscience and 1086 1087 Bioengineering 129:155–159. DOI: https://doi.org/10.1016/j.jbiosc.2019.09.002. Pasquina-Lemonche L, Burns J, Turner RD, Kumar S, Tank R, Mullin N, Wilson JS, 1088 1089 Chakrabarti B, Bullough PA, Foster SJ, Hobbs JK. 2020. The architecture of the Grampositive bacterial cell wall. Nature 582:294-297. DOI: 10.1038/s41586-020-2236-6. 1090 Patel H, Yadav VK, Yadav KK, Choudhary N, Kalasariya H, Alam MM, Gacem A, Amanullah 1091 M, Ibrahium HA, Park J-W, Park S, Jeon B-H. 2022. A Recent and Systemic Approach 1092 1093 towards Microbial Biodegradation of Dyes from Textile Industries. 14:3163. DOI: 1094 10.3390/w14193163. 1095 Peiris MMK, Fernando SSN, Jayaweera PM, Arachchi NDH, Guansekara TDCP. 2018. Comparison of Antimicrobial Properties of Silver Nanoparticles Synthesized from 1096 Selected Bacteria. Indian Journal of Microbiology 58:301-311. DOI: 10.1007/s12088-1097

018-0723-3.

1098

for the remediation of water. Journal of Cleaner Production 322:129051. DOI: 1100 https://doi.org/10.1016/j.jclepro.2021.129051. 1101 Rafique M, Rafique MS, Kalsoom U, Afzal A, Butt SH, Usman A. 2019. Laser ablation 1102 synthesis of silver nanoparticles in water and dependence on laser nature. Optical and 1103 Quantum Electronics 51:179. DOI: 10.1007/s11082-019-1902-0. 1104 1105 Rasheed A, Hussain S, Mushtaq W, Zubair M, Siddique K, Attia K, Khan N, Fiaz S, Azeem F, Chen Y. 2023. Application of silver nanoparticles synthesized through varying biogenic 1106 and chemical methods for wastewater treatment and health aspects. Environmental Science 1107 1108 and Pollution Research. DOI: 10.1007/s11356-022-24761-4. 1109 Raza S, Ansari A, Siddiqui NN, Ibrahim F, Abro MI, Aman A. 2021. Biosynthesis of silver 1110 nanoparticles for the fabrication of non cytotoxic and antibacterial metallic polymer based nanocomposite system. Scientific Reports 11:10500. DOI: 10.1038/s41598-021-90016-w. 1111 Robati D, Mirza B, Rajabi M, Moradi O, Tyagi I, Agarwal S, Gupta VK. 2016. Removal of 1112 hazardous dyes-BR 12 and methyl orange using graphene oxide as an adsorbent from 1113 1114 aqueous phase. Chemical Engineering Journal 284:687-697. DOI: https://doi.org/10.1016/j.cej.2015.08.131. 1115 Saeed S, Iqbal A, Ashraf MA. 2020. Bacterial-mediated synthesis of silver nanoparticles and 1116 their significant effect against pathogens. Environmental Science and Pollution Research 1117 27:37347-37356. DOI: 10.1007/s11356-020-07610-0. 1118 Saleh MN, Khoman Alwan S. 2020. Bio-synthesis of silver nanoparticles from bacteria 1119 Klebsiella pneumonia: Their characterization and antibacterial studies. In: Journal of 1120

Puri N, Gupta A, Mishra A. 2021. Recent advances on nano-adsorbents and nanomembranes

1099

Physics:

6596/1664/1/012115.

1121

1122

Conference

Series.

IOP

Publishing Ltd,.

DOI:

10.1088/1742-

1123	Sayyid NH, Zghair ZR. 2021. Biosynthesis of silver nanoparticles produced by Klebsiella
1124	pneumoniae. Materials Today: Proceedings 42:2045–2049. DOI:
1125	https://doi.org/10.1016/j.matpr.2020.12.257.
1126	Shahjahan M, Rahman MH, Hossain MS, Khatun MA, Islam A, Begum MHA. 2017. Synthesis
1127	and Characterization of Silver Nanoparticles by Sol-Gel Technique. Nanoscience and
1128	Nanometrology 3:34–39. DOI: 10.11648/j.nsnm.20170301.16.
1129	Simchi A, Ahmadi R, Reihani SMS, Mahdavi A. 2007. Kinetics and mechanisms of
1130	nanoparticle formation and growth in vapor phase condensation process. Materials &
1131	Design 28:850–856. DOI: https://doi.org/10.1016/j.matdes.2005.10.017.
1132	Singh P, Mijakovic I. 2022. Strong Antimicrobial Activity of Silver Nanoparticles Obtained by
1133	the Green Synthesis in Viridibacillus sp. Extracts. Frontiers in Microbiology 13.
1134	Singh A, Yadav VK, Chundawat RS, Soltane R, Awwad NS, Ibrahium HA, Yadav KK, Vicas
1135	SI. 2023. Enhancing plant growth promoting rhizobacterial activities through consortium
1136	exposure: A review. Frontiers in Bioengineering and Biotechnology 11. DOI:
1137	10.3389/fbioe.2023.1099999.
1138	Soltani S, Gacem A, Choudhary N, Yadav VK, Alsaeedi H, Modi S, Patel A, Khan SH, Cabral-
1139	Pinto MMS, Yadav KK, Patel A. 2023. Scallion Peel Mediated Synthesis of Zinc Oxide
1140	Nanoparticles and Their Applications as Nano fertilizer and Photocatalyst for Removal of
1141	Organic Pollutants from Wastewater. Water (Switzerland) 15. DOI: 10.3390/w15091672.
1142	Srinivasan R, Mathivanan K, Govindarajan RK, Uthaya Chandirika J, Govindasamy C. 2022.
1143	Extracellular synthesis of silver nanoparticles by bioluminescent bacteria: characterization
1144	and evaluation of its antibacterial and antioxidant properties. International Nano Letters
1145	12:169–177. DOI: 10.1007/s40089-021-00360-y.

- 1146 Sun SJ, Deng P, Peng CE, Ji HY, Mao LF, Peng LZ. 2022. Extraction, Structure and
- 1147 Immunoregulatory Activity of Low Molecular Weight Polysaccharide from Dendrobium
- officinale. *Polymers* 14. DOI: 10.3390/polym14142899.
- 1149 Swathilakshmi A V, Abirami S, Geethamala G V, Poonkothai M, Sudhakar C, Albasher G,
- 1150 Alamri O, Alsultan N. 2022. Phytonanofabrication of copper oxide mediated by Albizia
- amara and its photocatalytic efficacy. Materials Letters 314:131911. DOI:
- https://doi.org/10.1016/j.matlet.2022.131911.
- 1153 Tarekegn MM, Balakrishnan RM, Hiruy AM, Dekebo AH. 2021. Removal of methylene blue
- dye using nano zerovalent iron, nanoclay and iron impregnated nanoclay a comparative
- study. RSC Advances 11:30109–30131. DOI: 10.1039/D1RA03918K.
- 1156 Terzioğlu E, Arslan M, Balaban BG, Çakar ZP. 2022. Microbial silver resistance mechanisms:
- recent developments. World Journal of Microbiology and Biotechnology 38:158. DOI:
- 1158 10.1007/s11274-022-03341-1.
- 1159 Tripathi DK, Tripathi A, Shweta, Singh S, Singh Y, Vishwakarma K, Yadav G, Sharma S, Singh
- VK, Mishra RK, Upadhyay RG, Dubey NK, Lee Y, Chauhan DK. 2017. Uptake,
- 1161 Accumulation and Toxicity of Silver Nanoparticle in Autotrophic Plants, and
- Heterotrophic Microbes: A Concentric Review. Frontiers in Microbiology 8.
- 1163 Vimalanathan AB, Ernest V, Arumugasamy K, Tyagi MG. 2013. Biosynthesis of silver nano-
- particles by the bacterium Micrococcus luteus. International Journal of Applied Biology
- and Pharmaceutical Technology 4:77–83.
- 1166 Wang Z, Chen C, Liu H, Hrynshpan D, Savitskaya T, Chen J, Chen J. 2020. Enhanced
- denitrification performance of Alcaligenes sp. TB by Pd stimulating to produce membrane
- 1168 adaptation mechanism coupled with nanoscale zero-valent iron. Science of The Total
- Environment 708:135063. DOI: https://doi.org/10.1016/j.scitotenv.2019.135063.

- 1170 Wang L, Du Y, Zhu Q, Song J, Ou K, Xie G, Yu Z. 2023a. Regulating the Alkyl Chain Length
- of Quaternary Ammonium Salt to Enhance the Inkjet Printing Performance on Cationic
- 1172 Cotton Fabric with Reactive Dye Ink. ACS Applied Materials & Interfaces 15:19750-
- 1173 19760. DOI: 10.1021/acsami.3c02304.
- 1174 Wang Y, Yang L, Xu J, Xin F, Jiang L. 2023b. Applications of synthetic microbial consortia in
- biological control of mycotoxins and fungi. Current Opinion in Food Science 53:101074.
- DOI: https://doi.org/10.1016/j.cofs.2023.101074.
- 1177 Wang Y, Zhai W, Cheng S, Li J, Zhang H. 2023c. Surface-functionalized design of blood-
- 1178 contacting biomaterials for preventing coagulation and promoting hemostasis. Friction
- 11:1371–1394. DOI: 10.1007/s40544-022-0710-x.
- 1180 Wintachai P, Naknaen A, Thammaphet J, Pomwised R, Phaonakrop N, Roytrakul S, Smith DR.
- 1181 2020. Characterization of extended-spectrum-β-lactamase producing Klebsiella
- pneumoniae phage KP1801 and evaluation of therapeutic efficacy in vitro and in vivo.
- Scientific Reports 10:11803. DOI: 10.1038/s41598-020-68702-y.
- Wolf JB, Stawski TM, Smales GJ, Thünemann AF, Emmerling F. 2022. Towards automation of
- the polyol process for the synthesis of silver nanoparticles. *Scientific Reports* 12:5769.
- 1186 DOI: 10.1038/s41598-022-09774-w.
- 1187 Wypij M, Jędrzejewski T, Trzcińska-Wencel J, Ostrowski M, Rai M, Golińska P. 2021. Green
- 1188 Synthesized Silver Nanoparticles: Antibacterial and Anticancer Activities,
- Biocompatibility, and Analyses of Surface-Attached Proteins. Frontiers in Microbiology
- 1190 12.
- 1191 Yadav VK, Amari A, Wanale SG, Osman H, Fulekar MH. 2023. Synthesis of Floral-Shaped
- Nanosilica from Coal Fly Ash and Its Application for the Remediation of Heavy Metals
- from Fly Ash Aqueous Solutions. *Sustainability* 15:2612. DOI: 10.3390/su15032612.

1195	waste: Properties, mechanism of extraction and applications in environmental
1196	sustainability. Journal of Environmental Chemical Engineering 10:108550. DOI:
1197	https://doi.org/10.1016/j.jece.2022.108550.
1198	Yang J, Shojaei S, Shojaei S. 2022. Removal of drug and dye from aqueous solutions by
1199	graphene oxide: Adsorption studies and chemometrics methods. npj Clean Water 5:5. DOI:
1200	10.1038/s41545-022-00148-3.
1201	Yassin MT, Mostafa AAF, Al-Askar AA, Al-Otibi FO. 2022. Synergistic Antibacterial Activity
1202	of Green Synthesized Silver Nanomaterials with Colistin Antibiotic against Multidrug-
1202	Resistant Bacterial Pathogens. Crystals 12. DOI: 10.3390/cryst12081057.
1203	Resistant Dacterial Fathogens. Crystatis 12. DOI: 10.3370/Cryst12001037.
1203	Zaman Y, Ishaque MZ, Ajmal S, Shahzad M, Siddique AB, Hameed MU, Kanwal H,
1204	Zaman Y, Ishaque MZ, Ajmal S, Shahzad M, Siddique AB, Hameed MU, Kanwal H,
1204 1205	Zaman Y, Ishaque MZ, Ajmal S, Shahzad M, Siddique AB, Hameed MU, Kanwal H, Ramalingam RJ, Selvaraj M, Yasin G. 2023. Tamed synthesis of AgNPs for
1204 1205 1206	Zaman Y, Ishaque MZ, Ajmal S, Shahzad M, Siddique AB, Hameed MU, Kanwal H, Ramalingam RJ, Selvaraj M, Yasin G. 2023. Tamed synthesis of AgNPs for photodegradation and anti-bacterial activity: Effect of size and morphology. <i>Inorganic</i>
1204 1205 1206 1207	Zaman Y, Ishaque MZ, Ajmal S, Shahzad M, Siddique AB, Hameed MU, Kanwal H, Ramalingam RJ, Selvaraj M, Yasin G. 2023. Tamed synthesis of AgNPs for photodegradation and anti-bacterial activity: Effect of size and morphology. <i>Inorganic</i> Chemistry Communications 150:110523. DOI:
1204 1205 1206 1207 1208	Zaman Y, Ishaque MZ, Ajmal S, Shahzad M, Siddique AB, Hameed MU, Kanwal H, Ramalingam RJ, Selvaraj M, Yasin G. 2023. Tamed synthesis of AgNPs for photodegradation and anti-bacterial activity: Effect of size and morphology. <i>Inorganic Chemistry Communications</i> 150:110523. DOI: https://doi.org/10.1016/j.inoche.2023.110523.

1194 Yadav M, Dwibedi V, Sharma S, George N. 2022. Biogenic silica nanoparticles from agro-